INFLUENCE OF GLAZING ON THE PERFORMANCE OF FLAT PLATE SOLAR COLLECTOR

BY

AKEEF MURSYIDIY BIN MOHAMAD DAUD

A dissertation submitted in fulfillment of the requirement for the degree of Master of Science in Mechanical Engineering.

Kulliyyah of Engineering
International Islamic University Malaysia

NOVEMBER 2025

ABSTRACT

Although flat plate solar collectors are widely used, the effects of multiple glazing layers and varying glazing thicknesses on their thermal performance remain poorly understood. This study uses computational fluid dynamics (CFD) through ANSYS Fluent to determine the optimal glazing configuration that maximizes solar energy absorption while minimizing heat loss. The analysis is conducted in two stages: first by varying the number of glazing layers, and then by adjusting glazing thickness, focusing on absorber plate temperature, top heat loss coefficient, and useful heat gain. The configurations studied for the number of glazing layers are 1, 2, 3 and 4 layers. The parameters such as the area of the collector, the gap spacing between the absorber, glazing and successive glazing, and the boundary condition of each components of collectors are maintained consistently throughout the study. The configuration with 2 glazing layers yields the highest temperature absorber plate, while having the second highest top heat loss coefficient and rate of useful heat gain among the configurations studied. The configuration with 2 glazing layers is selected for further study of glazing thickness. The configurations studied for glazing thickness are 2 mm, 3 mm, 4 mm, and 5 mm. The 4 mm glazing thickness for the two-glazing-layer solar collector configuration yields the highest absorber plate temperature, matching the temperature observed in the two-glazing-layer configuration from the glazing number study, as both used the same 4 mm glazing thickness. The configuration of collectors with double glazing with 4 mm glazing thickness can be considered the most balanced configuration that allows for efficient thermal performance, in term of solar radiation transmittance between glazing and heat retention within the air gap. This highlights the importance of a well-balanced configuration in the flat plate solar collector's glazing, where a high absorber plate temperature can be achieved through trade-offs between thermal retention and energy output.

ملخص البحث

على الرغم من أن المجمعات الشمسية المسطحة تُستخدم على نطاق واسع، إلا أن تأثير عدد طبقات الزجاج وسُمكها المتغير على أدائها الحراري لا يزال غير مفهوم بشكل كافٍ. تهدف هذه الدراسة إلى تحديد التكوين الأمثل للزجاج الذي يحقق أقصى امتصاص للطاقة الشمسية مع تقليل الفاقد الحراري، وذلك باستخدام ديناميكيات الموائع الحسابية (CFD) من خلال برنامج .ANSYS Fluent. تُجرى التحليلات على مرحلتين: الأولى بتغيير عدد طبقات الزجاج، والثانية بتعديل سُمك الزجاج، مع التركيز على درجة حرارة صفيحة الماصّ، ومعامل الفقد الحراري العلوي، ومعدل الكسب الحراري المفيد .تمت دراسة تكوينات تتضمن طبقة واحدة، طبقتين، ثلاث وأربع طبقات زجاجية .وتم الحفاظ على ثبات المعاملات مثل مساحة المجمع، والمسافة الفاصلة بين الماصّ والزجاج، وكذلك بين الطبقات الزجاجية المتتابعة، وظروف الحدود لكل مكوّن من مكونات المجمع طوال الدراسة أظهرت النتائج أن التكوين المكوّن من طبقتين من الزجاج حقق أعلى درجة حرارة للماصّ، مع تسجيل ثاني أعلى معامل الفقد الحراري العلوي ومعدل الكسب الحراري المفيد بين التكوينات المدروسة. بناءً على ذلك، تم اختيار هذا التكوين لدراسة تأثير سُمك الزجاج بشكل أكثر تفصيلاً أما بالنسبة لسُمك الزجاج، فقد تمت دراسة تكوينات بسماكات 2مم، 3 مم، 4 مم، و5 مم .وأظهرت النتائج أن سُمك 4 مم في مجمع الطبقتين الزجاجيتين يحقق أعلى درجة حرارة للماصّ، وهي درجة الحرارة نفسها التي لوحظت في دراسة عدد الطبقات، حيث تم استخدام السُمك نفسه 4 مم ، يمكن اعتبار تكوين المجمع الشمسي ذي الطبقتين الزجاجيتين وبسُمك 4 مم هو التكوين الأكثر توازناً، إذ يحقق أداءً حرارياً فعالاً من حيث نفاذية الإشعاع الشمسي عبر الزجاج والاحتفاظ بالحرارة داخل فجوة الهواء .وهذا يبرز أهمية التوازن في تصميم الزجاج للمجمع الشمسي المسطح، حيث يمكن الوصول إلى درجة حرارة مرتفعة للماصّ من خلال تحقيق موازنة بين الاحتفاظ الحراري والإنتاج الطاقي.

APPROVAL PAGE

I certify that I have supervised and read this study and that in my opinion, it conforms to acceptable standards of scholarly presentation and is fully adequate, in scope and quality, as a dissertation for the degree of Master of Science in Mechanical Engineering.

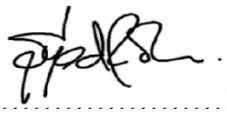

……
Syed Noh Syed Abu Bakar
Supervisor

……
Sany Izan Ihsan
Co-Supervisor

……
Mohd Azan Mohammed Sapardi
Co-Supervisor

I certify that I have read this study and that in my opinion it conforms to acceptable standards of scholarly presentation and is fully adequate, in scope and quality, as a dissertation for the degree of Master of Science in Mechanical Engineering.

……
Dr. Tengku Nordayana Akma Binti Tuan Kamaruddin
Examiner

……
Dr. Sa'adah Binti Ahmad @ Ahmad Sowi
External Examiner (If Applicable)

This dissertation was submitted to the Department of Mechanical and Aerospace Engineering and is accepted as a fulfilment of the requirement for the degree of Master of Science in Mechanical Engineering.

…….
Nur Azam Abdullah
Head, Department of Mechanical
and Aerospace Engineering

This dissertation was submitted to the Kulliyyah of Engineering and is accepted as a fulfillment of the requirement for the degree of Master of Science in Mechanical Engineering.

…….
Khairul Azami Sidek,
Dean, Kulliyyah of Engineering

DECLARATION

I hereby declare that this thesis is the result of my own investigations, except where otherwise stated. I also declare that it has not been previously or concurrently submitted as a whole for any other degrees at IIUM or other institutions.

Akeef Mursyidiy bin Mohamad Daud

Signature…… Date…18/8/2025……

INTERNATIONAL ISLAMIC UNIVERSITY MALAYSIA

DECLARATION OF COPYRIGHT AND AFFIRMATION OF FAIR USE OF UNPUBLISHED RESEARCH

INFLUENCE OF GLAZING ON THE PERFORMANCE OF FLAT PLATE SOLAR COLLECTOR

I declare that the copyright holder of this dissertation are jointly owned by the student and IIUM.

By signing this form, I acknowledged that I have read and understand the IIUM Intellectual Property Right and Commercialization policy.

Affirmed by Akeef Mursyidiy bin Mohamad Daud

…… Signature

18/8/2025 …….. Date

ACKNOWLEDGEMENTS

Allah, the Almighty, be praised for whose Grace and Mercies have been with me throughout the duration of undertaking this task. All of my might and willpower came from Him, for Allah S.W.T always guided me through the challenging time.

Thanks to my parents and my sibling for always thinking of me and wishing me well, even when I can't always be by their side. Their expectations and hopes fuel me to keep on working on this study and for that, they deserved my utmost gratitude. And thanks to my late grandmother, you will always be remembered throughout my life.

My gratitude goes to my supervisor, Dr. Syed Noh Syed Abu Bakar and co-supervisors Assoc. Prof. Dr. Sany Izan Ihsan and Dr. Mohd Azan Mohammed Sapardi for always guiding and correcting me during the study. I am so grateful for their support throughout my master's studies.

Lastly, thanks to everyone that directly or indirectly helped me during my master's degrees.

LIST OF CONTENTS

LIST OF TABLES

LIST OF FIGURES

LIST OF ABBREVIATIONS

CFD	Computational fluid dynamics
FPSC	Flat plate solar collector
P_r	Prandtl number
N_u	Nusselt number
T_p	Average temperature of absorber plate
T_g	Average temperature of glazing / glass cover
U_t	Top heat loss coefficient
Q_u	Useful energy gain
PV	Photovoltaic
HTF	Heat transfer fluid
R_a	Rayleigh number
T/T_o	Temperature profile

LIST OF SYMBOLS

σ	Stefan–Boltzmann constant
ε	Emissivity
g	Gravity
C_p	Specific heat capacity
k	Thermal conductivity

CHAPTER ONE

INTRODUCTION

1.1 BACKGROUND

The Earth's energy sources have been extensively explored and harvested since ancient times, including wood, natural gas, and solar energy. Fossil fuels have dominated due to their lower costs and convenience. As environmental pollution worsens from fossil fuel depletion, the search for alternative energy sources has intensified thus renewable and cleaner energy sources like wind, geothermal, and solar have emerged throughout the history (Barbier, 2002; Kannan & Vakeesan, 2016).

Wind energy, harvested by turbines, aids in agriculture and electricity production by utilizing solar energy's effect on Earth's surface temperature variations and it is a renewable source albeit with high initial and maintenance costs (Joselin Herbert et al., 2007). Geothermal energy is harvested from natural steam and hot water, is significant in countries near active plate boundaries and has grown in availability in the recent years (Huttrer, 2021). Solar energy is a abundant, clean, and eco friendly resource widely used in agriculture and everyday life. It is harnessed through technologies such as photovoltaic cells and solar thermal collectors, which convert sunlight into electricity and thermal energy, respectively.

Harnessing solar energy effectively requires careful consideration of several performance factors, including latitude, climatic conditions, and regional weather patterns. These factors play an important role in determining the accessibility and efficiency of solar thermal systems, and their consideration is essential for optimizing energy yield and ensuring economic viability (Klaiß et al., 1995; Tsoutsos et al., 2003).

Across the globe, many countries have adopted solar energy as a sustainable alternative to reduce dependence on non-renewable sources such as fossil fuels and coal, highlighting a growing shift toward cleaner and more renewable energy options.

Solar thermal collectors are typically categorized into stationary collector such as flat plate collectors (FPSCs), and sun tracking concentrating collectors. The FPSC is a system composed of an insulated metal casing, a transparent cover (usually glass) known as the glazing, and a dark absorber plate. These collectors are commonly installed facing the equator to maximize solar energy absorption (Barone et al., 2019; Kalogirou, 2004; Struckmann, 2008). The solar energy is transferred to a heat transfer fluid (HTF) such as water or air, inside tubes, enabling its use for the intended application.

There are many factors that affect the FPSC performance, such as absorber properties, angle and orientation, and heat transfer fluid selection (Lv et al., 2018; Shariah et al., 1999; Tsilingiris, 2002; Vignarooban et al., 2015). Glazing configurations such as number of layers and thickness also impact FPSC performance by influencing transmittance, reflectivity, and the shading effect (Chen et al., 2021; Nahar & Garg, 1980; O'Hegarty et al., 2016). While existing literatures have extensively covered the influence of glazing properties on FSPC performance, there remains a gap in understanding how factors such as the relation between the glazing number and the glazing thickness can affect the performance of FPSC. The purpose of this study is to study the effect of glazing number and glazing thickness on the performance of FPSC.

1.2 PROBLEM STATEMENT

Glazing is an important component of FPSC as it directly influences heat transfer within the system. Variations in the number of glazing layers and their thickness influence the absorber plate temperature (T_p) by altering the top heat loss coefficient (U_t), thereby impacting the outlet temperature and the useful energy extracted (Q_u). However, the specific effects of different glazing configurations on these performance parameters are not yet fully understood. This study addresses this gap by investigating how glazing configurations influence T_p, U_t, and Q_u, with the aim of optimizing FPSC design for improved thermal performance and reduced heat loss. This study focuses on investigating the impact of the number of glazing layer and thickness on the performance of FPSC, in terms of T_p, U_t, and Q_u. These FPSC parameters play a crucial role in enhancing the harnessing of solar radiation into usable heat. Addressing them enables the study to identify design improvements that can boost overall collector performance.

1.3 RESEARCH OBJECTIVE

The aim of this research is to investigate the influence of the glazing configurations on the thermal performance of the FPSC. The objectives of this study are:

1. to develop a benchmark FPSC model for simulation based on configurations from the literature review,

2. to evaluate the effect of the number of glazing layer on the average temperature of absorber plate, the top heat loss coefficient, and the rate of useful heat gain by FPSC, and

3. to evaluate the effect of glazing thickness on the the average temperature of absorber plate, the top heat loss coefficient, and the rate of useful heat gain by FPSC.

1.4 RESEARCH SCOPE

This study focuses on the studying the effects of glazing configurations on the thermal performance of FPSC using ANSYS Fluent software. The simplified 3-D model of FPSC only consists of absorber plate, glazing, insulator and casing. The dimension of absorber plate and the gap spacing between the absorber plate and glazing and successive glazing is maintained at the same distance. The inlet and outlet of fluid of FPSC is not considered in the simplified 3-D model of FPSC as the study focuses on the temperature of absorber plate only. The latitude and longitude of Kuala Lumpur, Malaysia will be used to simulate the solar radiation.

CHAPTER TWO

LITERATURE REVIEW

2.1 RENEWABLE ENERGY

Energy sources on Earth, such as wood, natural gas, and solar, have been explored since ancient times. Overconsumption and reliance on certain energy sources can harm the environment and human health. Historically, fossil fuels dominate due to their cost-effectiveness and convenience, but environmental concerns have grown recently. Consequently, efforts are underway to reduce dependence on depleting sources like natural gas and fossil fuels (Hoel & Kverndokk, 1996). There have been various alternative sources of energy that are renewable and cleaner that appear throughout the age of humanity such as, but not limited to, wind, geothermal and solar energy (Barbier, 2002; Joselin Herbert et al., 2007; Kannan & Vakeesan, 2016).

Wind energy is typically harvested from wind turbines and serves various purposes like agriculture and generating electrical power. This renewable energy source is indirectly powered by the sun through variations in the earth's surface temperature (Joselin Herbert et al., 2007). Despite its sustainability, wind energy requires substantial initial investment and maintenance costs (Njiri & Söffker, 2016).

On the other hand, geothermal energy, often in the form of natural steam and hot water, has long been used for electricity production and heating in many countries, especially those near active plate boundaries like the Pacific Ring of Fire and East African Rift System (Masum & Ali Akbar, 2019; Mutonga & Fujimitsu, 2024). In the 2020+1 World Geothermal Congress update report, Huttrer, (2021) reported that the

installed capacity has an increase of about 3.649 Gigawatt in the five-year term from 2015-2020, highlighting its growing traction as a renewable energy option worldwide.

2.2 SOLAR ENERGY

The solar energy has been utilized by humans for a very long time. Since the earliest age of humanity, humans are known to use sunlight for various purposes such as for the processes of drying of agriculture harvest and clothing where humans take advantage of the abundant source of energy emitted by the Sun which is clean and does not cause environmental pollution unlike other sources of energy (Bakari et al., 2014; S. O. Amiebenomo et al., 2013). It offers numerous advantages, including environmental friendliness, scalability, and independence from grid infrastructure. Harnessing solar energy involves various technologies, such as photovoltaic cells and solar thermal collectors, which convert sunlight into usable electricity and heat respectively.

There are many factors that need to be considered that can significantly affect solar energy availability such as latitude, climate conditions, and local weather patterns. The regions closer to the equator typically experience higher solar irradiance due to long daytime periods, making them good locations for solar energy harnessing. However, regions farther than the equator can also benefit from the solar thermal energy although the efficiency levels may differ due to shorter daytime periods. Hence understanding these influences is required to optimize the operation of solar thermal systems to maximize the energy yield and economic viability (Klaiß et al., 1995; Tsoutsos et al., 2003).

Tsoutsos et al., (2003) concluded in their study that industrial-scale solar thermal system can become a viable alternative on the electricity market, provided there is an adequate policy support and coordinated backing. Additionally, Klaiß et al., (1995)

stated that solar thermal power plants can have potential to become a viable in the future as long as there is a solid planning for the implementation of the solar thermal power plant while taking the factor of economic development, the existing infrastructure and electricity networks into the consideration.

Since solar energy offers a clean and renewable alternative, many countries across the globe have joined in the race to adopt and harness solar energy as a sustainable energy solution. According to the International - U.S. Energy Information Administration (EIA), it was reported that the electrical power generation has been steadily increasing across the world from 104 billion kWh in 2014 to 1280 billion kWh in 2022. This growth can be seen in the developed and developing nations alike, such as China, India, Germany, Mexico, and USA. This report shows that solar energy has become a more viable alternative source of energy in order to reduce dependency on non-renewable sources such as fossil fuels.

The heat from solar energy can be used to heat up indoor spaces such as houses and commercial building and for domestic hot water (Barone et al., 2019). Solar energy can help reduce the dependency on electricity for water heating, which is essential for tasks that require large amounts of hot water, such as laundry and dishwashing, especially in commercial and industrial building. Additionally, the thermal energy can be circulated through radiators or underfloor system to provide indoor space heating, enhancing energy efficiency (Echarri-Iribarren et al., 2019; Zeghıb & Chaker, 2015). These applications are especially effective in low to moderate-temperature climates, where they can greatly decrease dependence on conventional energy sources such as fossil fuels. In order to efficiently store and circulate the heat harvested by the solar thermal collectors, thermal energy storage systems and heat pump are used in conjunction with them (Kim et al., 2018; Y. Tian & Zhao, 2013).

However, the challenges of efficient and cost effective still prominent as indicated by Ukoba et al. (2024), Abidemi Obatoyinbo Ajayi et al., 2024) and Zhang et al. (2024). The challenges can include the public knowledge and awareness of solar energy as viable alternative energy sources, the insufficient proper infrastructure and financial planning as well as the reality of the economics of the place that planning to utilise the solar energy. The usage of land required was also brought up as one of the challenges as large area of land is needed for efficient energy generation while also competing with other uses such as urbanization and agriculture. The existing challenges calls for cooperation among involved organizations and government bodies as well as the public perception and demand to overcome it, ensuring that solar energy can be efficiently and reliably utilized as a key alternative energy source.

Ukoba et al. (2024) further emphasise implementing well-designed policies and financial incentives as to promote wider and faster adoption of solar energy in both residential and industrial sectors. Additionally, the improvement of solar energy technology, such as improved storage, grid infrastructure and climate resilience would be the one of the key in the transition to a sustainable energy future. By investing in these advancements, the enhancement of the efficiency and reliability of solar energy systems makes them more accessible and appeal to a broader range of users. This approach not only addresses current challenges but also paves the way for long-term environmental and economic benefits.

2.3 SOLAR THERMAL COLLECTOR

As technology has evolved over time, so too has the technology for harvesting solar energy progressed, leading to the development of numerous devices specifically

designed to harvest solar energy for various purposes. Nowadays, solar energy is often harvested using a device called a solar collector or solar thermal collector. These collectors are operated by converting the harnessed energy from the sun into useful heat, which is a key aspect of solar thermal technology. Do not mistake the solar thermal collector for a photovoltaic (PV) panel, even though both utilize solar energy. PV panel consists of a large amount of PV cells that contain many different semiconductor materials that are chained together to convert solar energy directly to electricity (Solar Photovoltaic Technology Basics | Department of Energy, n.d.).

In general, when sunlight hits a solar panel, the PV cells within the panel absorb the energy from the sunlight. This absorbed energy generates electrical charges that then move within the cell due to an internal electrical field, leading to the flow of electricity (Bayod-Rújula, 2019; Parida et al., 2011). In short, the PV panel specializes in directly generating electrical energy from solar energy. On the other hand, the solar thermal collector absorbs solar radiation and converts it into heat then transfers it using mediums such as air, water or heat thermal fluids that flow through the collector. The aspect of solar thermal collector will be explored in depth, covering its classification, efficiency, applications, and its utilities later in section 2.6.

Between solar thermal collectors and PV panels, especially the mono crystalline silicon-based module, there is stark differences in efficiency, ranging from 40% to 60% for solar thermal collectors and around 20% for the latter (R. Kumar & Rosen, 2011). In addition to higher production cost for PV panels, it is also much more sensitive to temperature, as its efficiency decreases significantly at higher temperatures compared to solar thermal collectors (El Alami et al., 2024). Many studies have been conducted to lessen the impact of this complications including various cooling methods to regulate the temperature of PV cells leading to developing hybrid photovoltaic thermal (PVT)

collectors (Herrando et al., 2023; Makki et al., 2015; Tiwari et al., 2023). Still, there remains a gap in optimizing these hybrid systems for large-scale deployment, balancing cost, thermal management, and long-term efficiency under real-world conditions. Moreover, few studies critically compare the trade-offs between the higher thermal efficiency of solar thermal collectors and the electricity-generating potential of PV systems in different climatic contexts, which is essential for informed technology selection.

Solar thermal collectors have garnered significant attention, as reflected by the growing number of scientific publications on solar thermal energy for power generation highlighting their potential for renewable energy harnessing, despite the sharp decline in global venture capital investment in 2022, after a steady rise in previous years, as shown in Figures 2.1(a) and (b) (Carlsson et al., 2024). In the same report, the European Commission's Joint Research Centre notes that solar heat market which utilizes solar thermal collectors for industrial processes, tripled globally, while countries such as Denmark showed strong growth in solar district heating between 2022 and 2023. The increasing focus on sustainability and the need to reduce greenhouse gas emissions have propelled research and development in solar thermal technologies. Solar energy stands out among other energy sources due to its cleanliness and the absence of environmental pollution in its reliance.

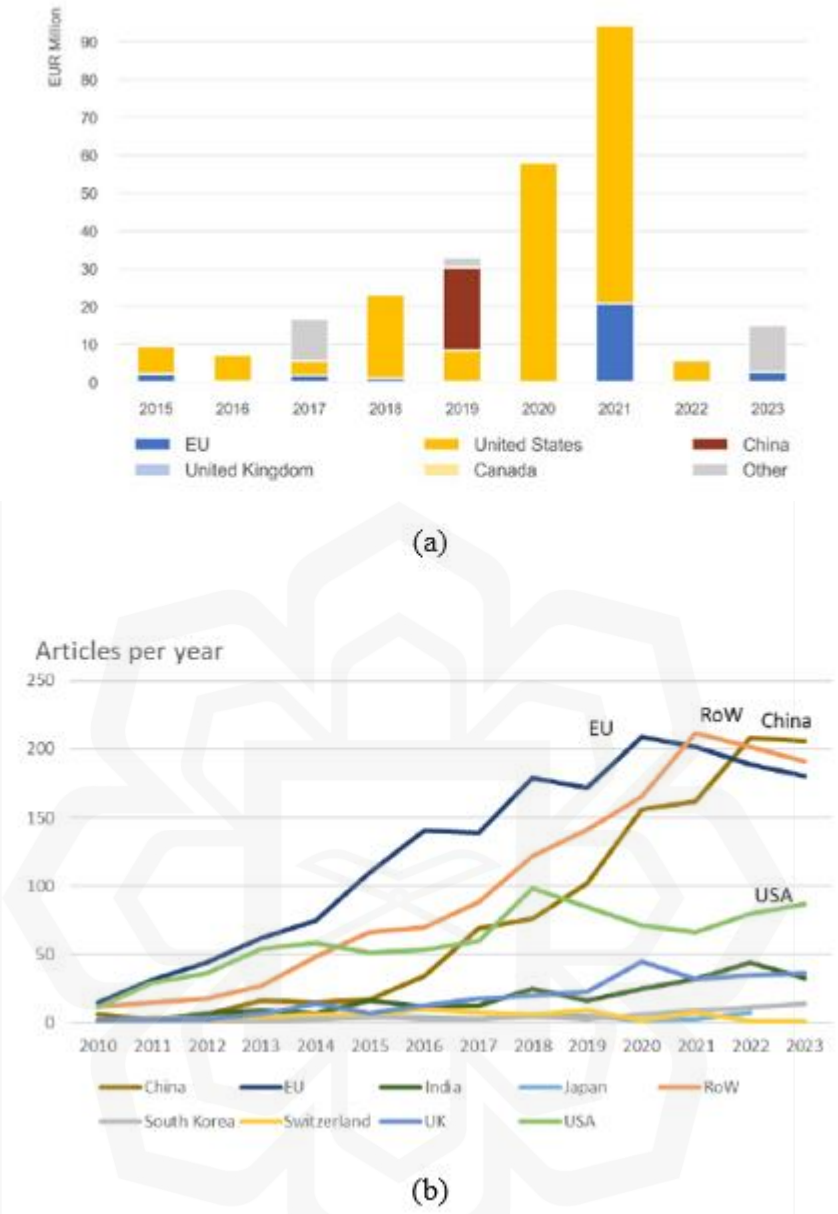

Figure 2.1 The trend of global venture capital investment by region (a) and scientific publications on solar thermal energy for power generation (b) (Carlsson et al., 2024).

2.4 SOLAR THERMAL COLLECTOR CLASSIFICATION

The solar thermal collector is designed to harvest the solar energy as efficiently as possible, so the design will vary from one collector to another collector. There are a variety of solar thermal collectors for residential or industrial-scale use that have different configurations to extract solar energy into heat energy. According to Kalogirou

(2004), solar energy collectors are primarily identified by their movement, which can be stationary, single-axis tracking, or two-axis tracking, along with the temperature at which they operate.

Kalogirou (2004) classifies the solar thermal collector into two different categories, stationary collectors and sun tracking concentrating collectors. There are three types of collectors that are grouped as stationary collectors: flat plate solar collectors (FPSC), evacuated tube collectors (ETC), and stationary compound parabolic collectors (CPC). These collectors remain stationary and do not follow the movement of the sun. For sun tracking concentrating collectors, solar energy is concentrated using optical before converting into heat. This concentration is achieved through mirrors or lenses, which reflect or refract solar radiation. The focused light is then concentrated in a specific area, boosting the energy flow toward the receiver.

There are four types of collectors that fall into this category: parabolic trough collectors (PTC), linear Fresnel reflector (LFR) and parabolic dish reflector (PDR). Barone et al., (2019), however classify the solar collectors into two types: non-concentrating collectors and concentrating collectors in which only FPSC and ETC is categorized as non-concentrating collectors and CPC, PTC, LFR and PDR falls into concentrating collectors, as illustrated in Figure 2.1.

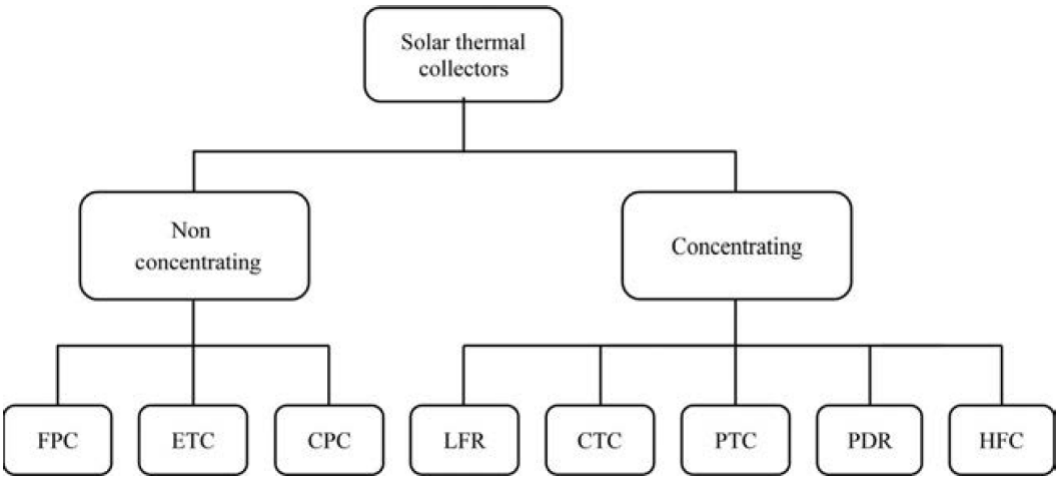

Figure 2.2 Barone et al.'s classification of solar thermal collectors (Barone et al., 2019).

A typical FPSC consists of an insulated metal enclosure with a transparent cover, usually made of glass or plastic, known as the glazing, along with a dark absorber plate and usually are installed facing the equator to absorb the as much solar energy as possible (Barone et al., 2019; Kalogirou, 2004; Struckmann, 2008). This glazing allows solar radiation to enter while minimizing heat loss. The absorber plate captures solar energy and converts it into heat, which is then transferred to a working fluid flowing through pipes attached to or integrated with the plate. These systems are valued for their simplicity and effectiveness in moderate-temperature applications such as domestic water heating (Chopra et al., 2021).

In contrast, CPC and ETC offer alternatives approaches in harvesting solar energy with improved efficiency in specific conditions(M. Tian et al., 2018). CPC features a reflective parabolic surfaces that reflects incoming solar radiation through multiple internal reflections due to its parabolic shape. The reflected radiation within the collector's acceptance angle is directed towards the absorber surface located at the base of the collector. This design allows them to capture diffuse and off-angle sunlight

within a certain acceptance angle, enhancing performance without the need for solar tracking (Jiang et al., 2020).

The ETC on the other hand, utilize the evaporation and condensation of the fluid inside of sealed glass tubes containing heat pipes. The fluid undergoes a phase change, evaporating at the hotter end of the heat pipe or evaporator and condenses at the cooler end or condenser, thereby transferring the thermal energy (Kalogirou, 2004). This method provides excellent thermal insulation and efficiency, particularly in colder climates (A. Kumar et al., 2020). The advantages of stationary collector are the simpler design, reliability, and cost-effectiveness, which make them well-suited for use in residential applications.

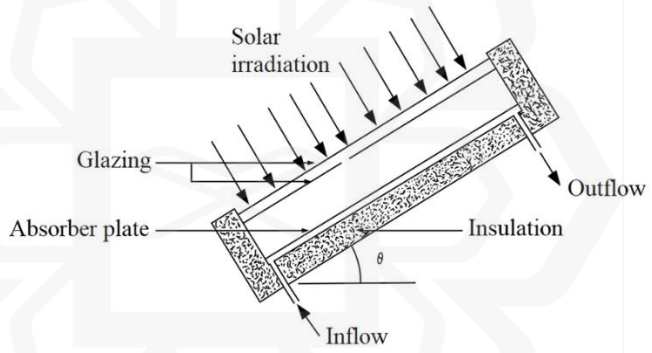

Figure 2.3 Schematic diagram of a flat plate solar collector (Mesa F., 2006).

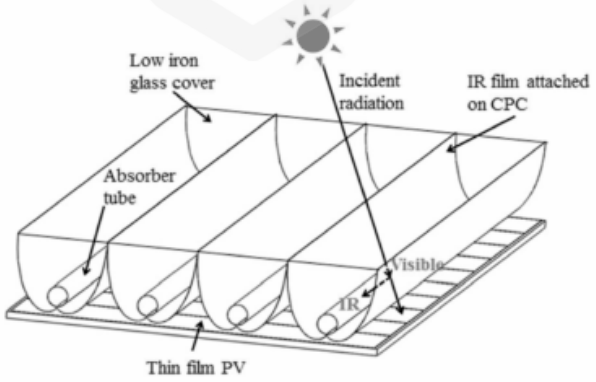

Figure 2.4 Schematic diagram of a compound parabolic collectors with a hybrid photovoltaics system (Jiang et al., 2020).

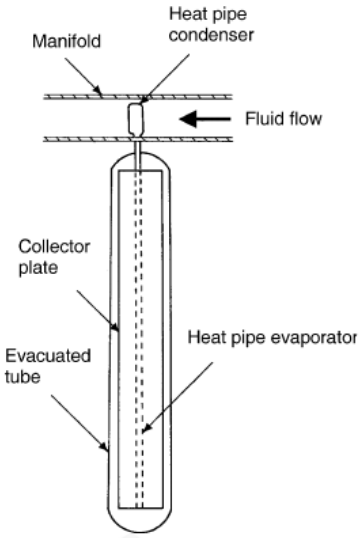

Figure 2.5 Schematic diagram of an evacuated tube collector (Kalogirou, 2004).

For concentrating collectors, it utilizes a tracking system to adjust the tilt angle and orientation of the solar collector panel to track the Sun's orientation continuously and precisely throughout the years because of concentrating or focusing the solar radiation into the focal point of collectors. This allows the concentrating collector to increase the amount of energy extracted from solar radiation by decreasing the area where the heat losses occur (Kalogirou, 2004). The PTC normally uses this system to heat up the solar receiver at the focal point of the parabolic shaped reflector. The receiver of a PTC typically comprises a fluid-filled tube positioned along the focal line of the reflector, where it absorbs the solar radiation. The LFR also uses this tracking system as an improvement where this technology utilizes an arrangement of sun-tracking linear mirror strips to focus sunlight onto a stationary receiver mounted on a linear tower.

The PDR uses the focal point of the dish to concentrate the solar energy onto a receiver while tracking the Sun orientation to maximize the absorption of radiant solar energy. In summary, concentrating collectors represent a cutting-edge approach to solar energy capture, having significantly higher efficiencies compared to non-concentrating

collector and the ability to generate high temperatures ideal for specialized applications such as industrial processes and power generation for bigger. The innovative design for maximizing solar radiation harnessing makes them a promising solution for meeting the growing demand for sustainable energy sources in various sectors.

While stationary collectors such as FPSCs and ETCs are widely adopted due to their simplicity and lower cost, their efficiency is inherently limited by their fixed orientation and inability to concentrate on solar radiation (Faddouli et al., 2024; Ismoilov et al., 2024). In contrast, sun-tracking concentrating collectors achieve higher efficiencies by focusing sunlight onto a smaller absorber area, but they are mechanically complex, more expensive, and highly dependent on direct sunlight, making them less suitable in regions with high cloud cover or diffuse radiation (Li et al., 2024; C. Zhang et al., 2024). This trade-off between simplicity, cost, and efficiency remains a key consideration in selecting solar thermal collectors for different applications. Despite the higher thermal efficiency of concentrating collectors, their widespread adoption is constrained by mechanical complexity, maintenance requirements, and the high initial investment, highlighting a persistent gap between potential efficiency and practical deployment.

Compared to other types of solar thermal collectors, FPSC generally offer lower thermal efficiency, especially against concentrating and tracking collectors. However, their widespread use in residential applications is attributed to their simple design, proven reliability, and low installation and maintenance costs. These features make FPSCs a practical and accessible choice for domestic uses such as water heating, especially in regions with moderate climates where high-performance systems may not be necessary (Duffie & Beckman, 2013).

2.5 FLAT PLATE SOLAR COLLECTOR (FPSC)

The FPSC is a commonly and commercially available solar thermal collector and it can be seen normally installed on residential and industrial buildings. Many of the FPSC are used to collect the solar energy and convert it to thermal energy that can be useful for many purposes, especially in heating the house, water or generating electricity. As stated before in Section 2.5, a normal FPSC is an insulated metal enclosure containing a dark-colored absorber plate and a glass or plastic covering known as glazing where the collector can heat the liquids or air in a condition where the temperature is below 80°C (Struckmann, 2008).

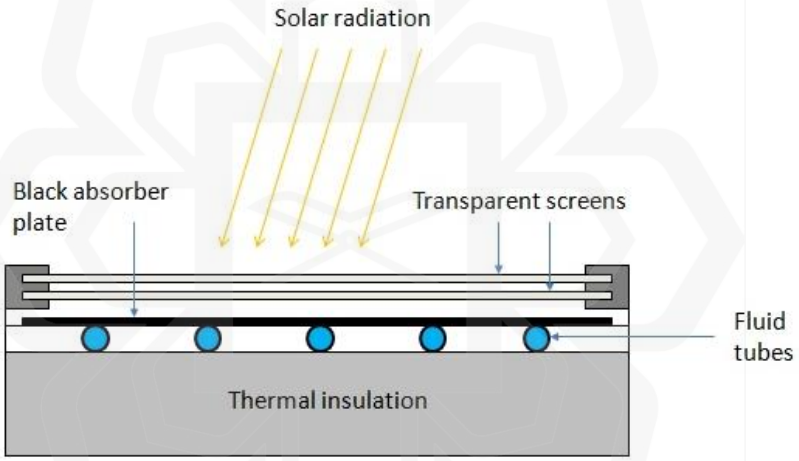

Figure 2.6 The schematic diagram of a flat plate solar collector showing key components for capturing and transferring solar energy (Witmer & Fedkin, n.d.).

FPSC shown in the Figure 2.4 demonstrates how the solar radiation is captured by utilising key components such as absorber plate, glazing or transparent screen, fluid tubes and insulator. Incoming solar radiation first penetrates the glazing layers, which serve to reduce convective and radiative heat loss while allowing light to pass through. The dark absorber plate located below the glazing, designed with high thermal conductivity and absorptivity to efficiently convert solar radiation into heat (Kalogirou, 2004). Beneath the absorber lie the fluid tubes, which carry the heated medium that

usually contain flowing water or heat transfer fluid throughout the collector system. To boost efficiency further, a substantial layer of thermal insulation is added at the base of the collector to minimize heat loss downward. This setup ensures effective collection and retention of solar thermal energy, making it ideal for uses such as water heating and space heating in both residential and commercial settings.

The liquid tube or fluid tube, where the transport medium flows to transfer the thermal energy from the absorber, can be configured into two layouts which are header/risers and serpentine configurations as shown in Figure 2.5 and Figure 2.6, respectively (Barone et al., 2019). For header and riser configuration, liquid tubes are connected to the large diameter header tube at both ends where the cooler liquid enters and hotter liquid exits. For serpentine configuration, the liquid tubes are arranged in a continuous, winding pattern across the absorber plate. The liquid tubes can be either an integral part of the absorbing plate itself or even welded to the plate.

The header/riser configuration, as shown in Figure 2.5, features two larger diameter of horizontal headers (inlet and outlet) linked by several parallel riser tubes. The bottom header is where the cold fluid enters the FPSC, flowing through the parallel risers to distribute the heat and lastly exit through the upper header as hot fluid. This configuration supports natural thermosiphon circulation, where the thermosiphonic effect occurs as solar radiation heats the water or heat transfer fluid in the collector, causing it to expand, become less dense, and rise into the top of the storage tank. Cooler, denser water from the bottom of the tank then flows down to replace it, maintaining continuous circulation as long as solar energy is available (Kalogirou, 2014). The header/riser configuration also can use suitable pump for forced fluid circulations inside the tubes. For serpentine configuration, the use of forced circulation via pump is recommended due to the higher pressure losses taking place inside the tube.

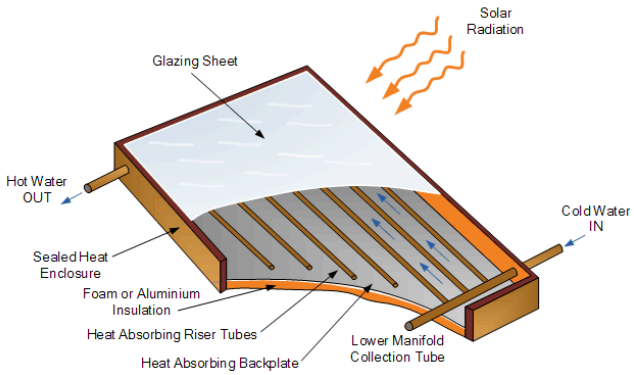

Figure 2.7 The schematic diagram shows the internal components and working principle of a Flat Plate Solar Collector with header/risers configurations (Alternative Energy Tutorials, n.d.).

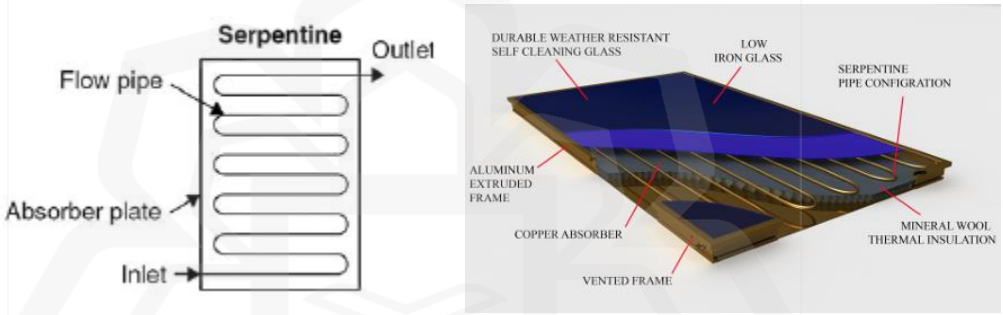

Figure 2.8 The simplified 2-D top-down schematic diagram of FPSC with serpentine configuration showing basic layout and components (left) (Barone et al., 2019) and detailed 3-D schematic illustration highlighting structural configuration and arrangement (right) (National Standards Authority of Ireland (NSAI), 2011).

For the glazing, its purpose is to reduce the heat convection loss from the absorber plate as the glazing traps a stagnant layer of air between the absorber plate and the glass, while also reducing radiation losses by greenhouse effect. The FPSC normally are installed facing the equator directly, pointing south in the northern hemisphere and north in the southern hemisphere. The ideal tilt angle for the FPSC matches the latitude of the area, with slight adjustments. Each of these elements can directly affect the efficiency of FPSC with a varying level of impact on heat retention, solar absorption, and overall thermal performance.

2.6 FLAT PLATE SOLAR COLLECTOR PERFORMANCE FACTOR

The performance of FPSC is an important aspect in evaluating the effectiveness and efficiency of solar energy utilization. The factors that can influence the performance of FPSC in terms of efficiency will be discussed in this chapter. The factors that influence the efficiency of FPSC are the absorber and its properties such as material and coating, HTF, tilt angle and orientation of FPSC and glazing properties (Barone et al., 2019).

2.6.1 The Absorber of FPSC

The absorber plate of FPSC should maximize the absorption of irradiation through the glazing while minimizing heat loss both upwards to the atmosphere and downwards through the back of the casing or insulator, as it is the component where the most heat transfer occurs (Kalogirou, 2004). Typically, absorber plates are made from material with high thermal conductivity such as aluminium, copper and steel in order to increase the rate of heat transfer (Shariah et al., 1999; Tsilingiris, 1999, 2002). Shariah et al., (1999) found that copper which has the highest thermal conductivity improve the performance the most compared to the aluminium and steel, but Shariah et al., (1999) also pointed out that copper offer no additional benefit compared to the aluminium as they mentioned that copper only increase the annual solar fraction by about 1% when compared to the aluminium. Another study by Sup et al., (2014) shows that aluminium has higher water heating efficiency value compared to the copper. This finding, which contradict with the by Shariah et al., (1999), is explained by Sup et al., (2014), who stated that copper has higher thermal conductivity compared to the aluminium, but aluminium has higher heat retention capability compared to copper. Aluminium can be regarded as a good absorber material for FPSC due to its high thermal conductivity, ability to retain heat longer and lower cost.

The optimal absorber coating should enhance solar absorption and transmission while minimizing reflection, using antireflective coatings and surface texture (Moncada et al., 2014; Sakhaei & Valipour, 2020; Senthil et al., 2021). Carbon coatings, known for high absorption and light-trapping abilities, improve thermal efficiency compared to black-painted absorbers (Sakhaei & Valipour, 2020). Studies show that carbon-coated and black chrome-coated absorbers have higher thermal efficiency than black-painted ones, with graphene coatings also outperforming black paint (Senthil et al., 2021). Additionally, epoxy coatings are superior to commercial absorbers, highlighting those materials with low reflectivity and high absorptivity, like carbon and epoxy, enhance solar collector performance (Moncada et al., 2014).

2.6.2 The Tilt Angle and Orientation of FPSC

The efficiency of FPSCs can be influenced to varying degrees by their tilt angle and orientation (Kocer et al., 2015; Lv et al., 2018; Morcos, 1994; N'Tsoukpoe, 2022). These factors determine the amount of solar radiation that the collector surface receives, which directly impacts the thermal efficiency and overall energy yield. Lv et al. (2018) and N'Tsoukpoe, (2022) concluded slight deviation from the optimal orientation have a negligible impact on incident solar radiation, thus barely affect the energy production. N'Tsoukpoe, (2022) reported that in West and Central Africa, a moderate adjustment of up to 20° from the ideal orientation and tilt angle does not significantly impact solar production. Lv et al., (2018), from their study in Lhasa, China, suggested that it is not recommended to change the optimum tilt angle every month during the heating season because adjusting the optimum tilt angle on a monthly basis does not notably affect the maximum hourly average total effective solar heat collection compared at fixed angle.

On the other hand, Morcos (1994) found that there is a noticeable increase in the total solar irradiation when the tilt angle of FPSC is adjusted several times a year. This finding is supported by Kocer et al., (2015) where they concluded that that there is noticeable energy loss when the flat plate collectors are tilted using the yearly average fixed angle when compared to the monthly optimum tilt. The studies conducted by Morcos (1994) and Kocer et al., (2015) illustrate that optimizing the orientation of the solar collector to face the sun throughout the year results in enhanced efficiency of the solar collector. The results of various research papers on tilt angle and orientation present conflicting findings, shows a contradiction in the conclusions reached by different studies which can be due to variations in geographic location where the research was conducted, influencing solar exposure and climatic conditions.

2.6.3 The Heat Transfer Fluid (HTF) of FPSC

The HTF plays a crucial role in various thermal systems and processes, serving as the medium through which heat is transferred from the absorber to the intended application and can impact on the overall performance, efficiency, and reliability of FPSC. Desired properties for HTF can include but are not limited to high thermal conductivity, high boiling point, high heat capacity, low melting point, low viscosity, and low cost (Vignarooban et al., 2015). The HTFs can be categorized into six primary groups depending on the material type: gases including air and others, water or steam, thermal oils, organic compounds, molten salts, and liquid metals (Elcioglu et al., 2020; Vignarooban et al., 2015; Vutukuru et al., 2019; Yoo et al., 2007). For households FPSC that operate on low temperature, water is predominantly used due to its effectiveness in absorbing and transferring thermal energy, cost efficiency, and widespread availability (Barone et al., 2019).

The HTF flow, whether laminar or turbulent, impacts the thermal efficiency of flat plate solar collectors. Adding nanoparticles to water can enhance this efficiency, especially in turbulent flow, which promotes better mixing and heat distribution, theoretically increasing the rate of heat transfer. Turbulent flow increases the contact area between the fluid and the heat transfer surface, facilitating more effective heat transfer (Elcioglu et al., 2020; Genc et al., 2018; Gupta et al., 2015). Elcioglu et al., (2020) reported that turbulent flow exhibits higher thermal efficiency compared to laminar flow, but this efficiency decreases as nanoparticle fractions increase due to the pumping power penalty.

Genc et al., (2018) supported this finding, stating that higher water flow rates resulted in higher thermal efficiency due to a transition from laminar to turbulent flow regimes. Gupta et al., (2015) concluded in their study that the water flow rate at 2.5 litre per minute is optimum for maximum collector efficiency. In conclusion, the flow regime of the heat transfer fluid (HTF) is crucial for the thermal efficiency of flat plate solar collectors as turbulent flow typically enhances heat transfer by improving mixing and increasing contact area with the heat transfer surface.

2.6.4 The Effect of Glazing on FPSC

Glazing refers to the layer that is added on top of the flat plate solar thermal collector which is usually made from transparent materials, such as glass or plastic. Glazing is a critical component of FPSCs, serving protective and thermal functions. It protects the absorber and other internal components from environmental exposure while reducing heat loss by limiting convective and radiative losses through the top surface (Kalogirou, 2004; O'Hegarty et al., 2016). However, the glazing also affects the optical transmittance of solar radiation or short-wave radiation. Therefore, an optimal glazing

design must balance improved thermal insulation with minimal optical losses (Akhtar & Mullick, 1999; Ehrmann & Reineke-Koch, 2012; Giovannetti et al., 2014; Khoukhi et al., 2006).

Additionally, the greenhouse effect can occur inside FPSC once the glazing layer is introduced, as it also traps and re-radiates back some of the thermal (long-wave) radiation emitted from the absorber plate, and the inner glazing effectively redirects more energy back toward the absorber. This phenomenon can affect the surface incident radiation on the absorber plate and glazing as additional glazing layers are introduced (Patrick et al., 2019).

2.6.4.1 The Effect of the Number of Glazing Layer

The glazing number refers to the amount of glazing installed above the absorber plate in the FPSC. Most of the FPSC consist of one glazing layer, where there is a single glazing or glass cover that enclosed the upper casing of FPSC. The glazing number also can affect the performance of solar thermal collectors as observed by Ihaddadene et al., (2014), where they performed a study regarding the effect of the glazing number on the solar thermal collector performance. They performed the testing on an active solar energy demonstration system called ET200 which consist of FPSC, water storage tank, control panel and lamp to simulate natural sunlight. It was observed that adding an additional glazing layer with the same thickness on top of the FPSC decreases the water temperature difference between the inlet and outlet of the absorber decreases, thus decreasing the efficiency of the solar collector. The gap spacing between the absorber plate, first glazing and second glazing, however, was not mentioned except the additional glazing layer is placed 2-cm above the FPSC. Ihaddadane et al. (2014) explained that having more glazing layers creates more air layers between the heat

source and the water. As the air layers act as thermal insulators, the energy transmitted from the heat source to the water decreases as less energy being transmitted between the glazing layers.

Al-Ajlan et al., (2003) briefly discussed the effect of glazing number on the FPSC performance in Riyadh. They found that more glazing layers lowered the collector's optical efficiency as each extra pane reflects or absorbs a fraction of the incoming short-wave radiation before it reaches the absorber. The optical efficiency is defined by the ratio of the rate of optical or short wavelength energy that reaches absorber or receiver to the incident solar radiation (Sukhatme, 2009). However, they also noted that at moderate operating temperature, the reduction heat loss through convection and reradiation of multiple glazing layers will outweigh the decrease of optical efficiency. Here, the operating temperature is referred to the temperature of the HTF. As a result, the FPSC with two layers configurations will have higher peak outlet temperatures despite a small drop in optical efficiency at moderate operating temperature.

A study has been conducted by Chen et al. (2021) in order to investigate how well double-glazed flat-plate solar air collectors perform under conditions of low ambient temperature and high inlet temperature in terms of thermal performance. The settings of flat-plate solar air collectors that were tested are single glazing, double glazing filled with air, double glazing filled with argon and double glazing with vacuum. They concluded that the configurations other than single glazing have better thermal performance due to reduced convection heat transfer compared than the single glazing. However, they only examined the effect of two glazing layer with the air gap between

them, leaving a notable gap in understanding the effect of having more than two glazing number especially on the thermal efficiency of FPSC.

2.6.4.2 The Effect of the Thickness of Glazing

The glazing thickness also can affect the performance of FPSC since it can affect the solar radiation transmittance and reflectivity (Bakari et al., 2014; Liu et al., 2022). According to Bakari et al., (2014), 4-mm thickness glazing give better performance compared to 3-, 5- and 6-mm glazing thickness for fruit drying, as 4-mm glazing thickness provide optimal balance between solar transmittance and reduced convective losses. Their results showed that a 3-mm glass thickness results in high transmittance (low reflectivity) but also high convective losses, leading to poorer performance compared to 4mm glass. Conversely, although 5-mm and 6-mm glass thicknesses exhibit lower convective losses, they also exhibit a low transmittance (high reflectivity) which results in poorer performance relative to 4mm glass. Thus, a 4-mm glazing thickness provides the optimal balance of transmittance and convective losses, making it the best choice for glazing thickness.

This result is supported by Liu et al., (2022) where a study on the effect of glazing thickness on corrugated FPSC and they concluded that that 4-mm yield the highest maximum heat collection efficiency followed by 8-mm and finally 6-mm. They concluded that increasing the glass thickness can diminish radiation intensity due to the insulation properties of the glass and the 8-mm glazing thickness makes the insulation effect of the glass more pronounced. The studies show that thinner glazing, most notably 4-mm thickness is better for the FPSC due to the reduced insulating effect of the glass, resulting in less reduction in radiation intensity. However, all of the mentioned studies

on glazing thickness only examine the effect of glazing thickness for single glazing, neglecting the potential impacts that might occur with multiple glazing layers.

2.6.4.3 The Gap Spacing of Glazing

The space between the absorber and the cover glazing, as well as between successive layers of cover glazing, is crucial in FPSC design and efficiency. The performance of FPSC is influenced by several parameters related to the air gap, including natural convection and the shading effect on the absorber caused by side walls (Nahar & Garg, 1980; Nahar & Guf'ta, 1989). According to Nahar & Guf'ta, (1989) it is recommended to maintain a 50-mm air gap between the absorber plate and the cover glazing, as well as between successive glazing layer, in FPSC when it is compared to 25-mm and 150-mm. This is due to the effect of the shading and the convective loss for 50-mm air gap is minimum compared to the other gap. This finding is supported by another study by Nahar & Garg, (1980) where it is recommended that a gap of 40-mm to 50-mm should be maintained for the least effect of shading and convection loss. So, 50-mm can be the most suitable air gap distance between the absorber and the glazing and the successive glazing layer.

2.6.4.4 The Optical Properties of Glazing

The glazing itself can affect solar energy reaching the absorber plate due to its key properties such as emissivity, transmittance, reflectivity and absorptivity of solar irradiation. Optimally, the glazing is recommended to have high transmittance, low emissivity to allow more solar energy to reach the absorber while reducing its loss to surrounding (Fan & Bachner, 1976.; Goodman & Menke, 1975).

Emissivity is the ratio of the radiation emitted by a surface such as the outer surface of glazing at a specific temperature, compared to the radiation emitted by a

blackbody at the same temperature, while transmittance refers to the ratio of transmitted radiation or radiation that passes through the glazing compared to the irradiation (Cengel & Ghajar, 2014). For commercial FPSC, glazing is normally layered with silver coating, that provide very low emissivity, less than 0.03 and solar transmittance of mostly below 0.60 (Giovannetti et al., 2014). For reflectivity and absorptivity, both should ideally be minimized to reduce unwanted heat losses and improve the thermal efficiency of the system (Bakari et al., 2014). Figure 2.7 shows how the absorption, reflection and transmittance of incident radiation occur on the semitransparent material such as glass.

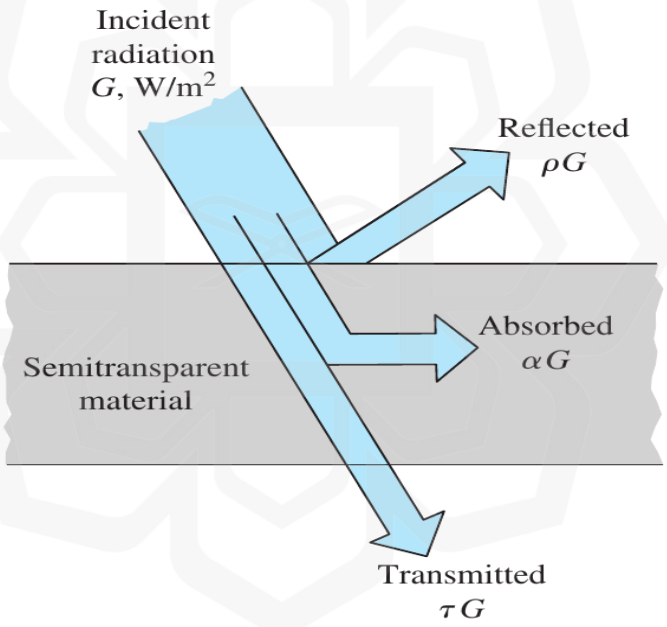

Figure 2.9 the optical properties of semitransparent materials *(Cengel & Ghajar, 2014)*.

The glazing can be improved by using the anti-reflection coating such as magnesium fluoride (M_gF_2) coating (Hsieh & Coldewey, 1974) and porous sol-gel coating (Khoukhi et al., 2006) to minimize the energy loss by reflection on the outer surface of the glazing. Additionally, using low emissivity (low-e) glass or coating,

which fall under the category of spectrally selective materials, can help to minimize the radiation losses to the surrounding while simultaneously increasing the solar energy transmission to the absorber plate (Giovannetti et al., 2014). Both improvement can be utilised as shown by (Hammarberg & Roos, 2003), where they used the thin film of silicon dioxide (SiO_2) on both side of glazing to further improve the transmittance while reducing the reflection and emissivity of the glazing.

The absorptivity of glazing also can affect the performance of FPSC, since the glazing can absorb the irradiance from the Sun, the infrared (IR) radiation re-emitted by the absorber plate and other glazing, causing greenhouse effect to occur within FPSC, improving the thermal efficiency by trapping the heat thus heating up the FPSC (Jannot & Coulibaly, 1997). Although glazing with higher absorptivity can promote heat trapping from greenhouse effect, it also leads to greater convection and radiation losses as the glazing temperature rises (Akhtar & Mullick, 2012). So, to resolve this tradeoff, the glazing can utilise the spectrally selective coatings that reflect the IR radiation back to the absorber to decrease the thermal losses on the glazing while allowing short-wave solar radiation to pass through and heats up the absorber plate while decreasing the temperature of glazing (Giovannetti et al., 2014).

The amount of heat energy from solar irradiance that is transmitted, absorbed, and reflected through the glazing also can be affected based on the number of glazing layers and glazing thickness. As stated before in 2.6.4.1, Ihaddadene et al. (2014) concluded that double glazing reduced the radiation energy transmitted to the absorber plate thus decreasing heat energy absorbed. Bakari et al., (2014) concluded in their study that the thicker the glazing is, the lower the transmittance and the higher the reflectivity of the glazing will be. For optimum optical properties of glazing on FPSC, it should have high transmittance, low emissivity, low reflectivity and low absorptivity.

2.7 SUMMARY

It is important to remember that heat transfer within the FPSC is significantly affected by the factors mentioned, therefore, these factors must be considered when designing an efficient FPSC. This study will focus on the effect of glazing properties, specifically, the number of glazing layers and thickness. While previous studies have explored how these properties affect FPSC performance, there are still gaps in understanding the optimal glazing number and thickness for FPSC performance. Even though there are studies that focus on either the number of glazing layers or their thickness, most of them examine only one of these configurations without considering the combined effect of both. Selection of the optimal number of glazing layer and glazing thickness requires careful consideration in FPSC design. Addressing these gaps through focused research can lead to improvement in designing more efficient FPSCs.

CHAPTER THREE

RESEARCH METHODOLOY

3.1 INTRODUCTION

This chapter outlines the approach used to address the problem presented in Chapter 1. The flow chart of the methodology is shown in Figure 3.1. Firstly, the literature review focusing on the FPSC studies is performed. Then an FPSC benchmark FPSC configuration is developed. In validating the CFD model, the work of Subiantoro & Ooi (2013) and Wang et al. (2017) are used. After successful comparison and validation, the study proceeds to investigate the effect of the number of glazing layers, which includes configurations with 1-, 2-, 3-, and 4- glazing layers. Then the best configuration of the number of glazing layers will be further studied with the configuration of the glazing thickness, ranging from 2-mm to 5-mm. The results will be analyzed, discussed and reported.

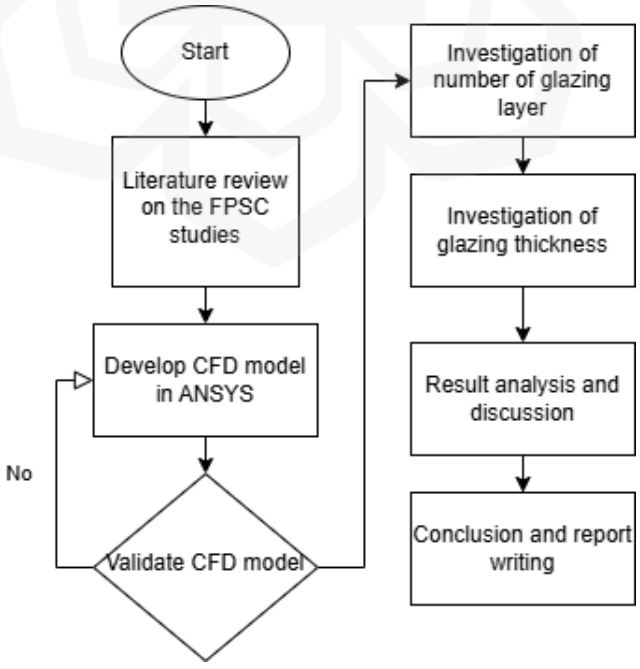

Figure 3.1 The flow chart of the study.

3.2 FPSC BENCHMARK CONFIGURATION BASED ON LITERATURE REVIEW

The details of the FPSC benchmark configuration will be established based on the extensive review of relevant literature, aiming to identify commonly adopted design features, material selections, and operating conditions that represent a standard configuration of FPSC for performance comparison. The scope of this study focuses on the top part of the FPSC, therefore only the components from the absorber plate up to the glazing are included in the simulation.

The illustration of the created physical domain for this study is shown in Fig. 3.2. The size of the physical domain for the 1-glazing configuration is 500-mm length × 300-mm width × 74-mm height, consisting of glazing, air and absorber plate. The glazing and absorber plate thicknesses are 4-mm and 20-mm, respectively. The gap between the absorber plate and glazing is 50 mm. The length and width of the absorber plate, air gap and glazing are the same. For 2-, 3- and 4-glazing configurations, the gap spacing and the glazing thickness are added accordingly, while the dimension is maintained as the gap spacing and glazing thickness for 1-glazing configuration. The geometrical parameters of the domain from Fig. 3.2 are tabulated in Table 3-1 with their values.

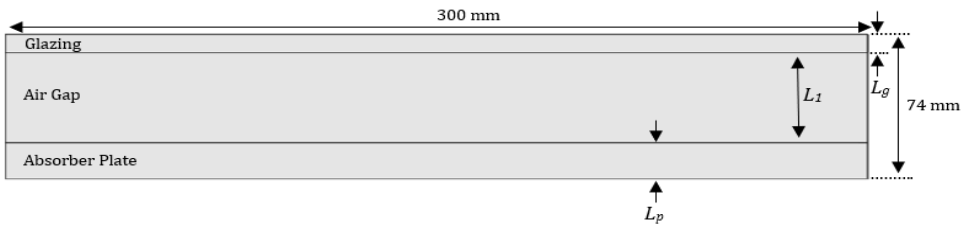

(a)

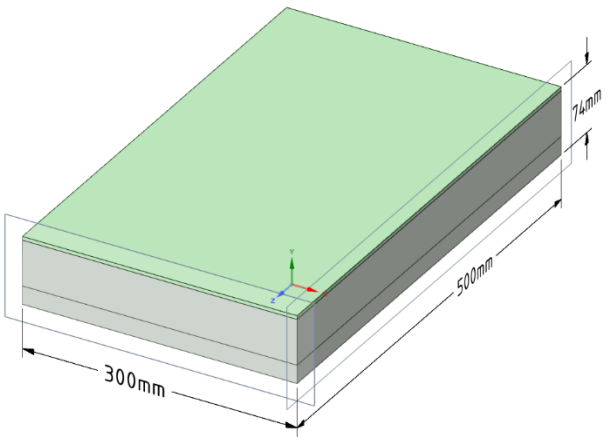

(b)

Figure 3.2 Physical domain for 1 glazing layer. (a) is the front view of the domain and (b) is the isometric view of the domain.

Table 3-1 The geometrical parameters for the top part of FPSC model.

Geometrical Parameters	**Value**
Glazing thickness, L_g	4-mm
Absorber plate thickness, L_p	20-mm
Air gap spacing between absorber plate and first glazing, L_1	50-mm
Air gap spacing between first glazing and second glazing, L_2	50-mm
Air gap spacing between second glazing and third glazing, L_3	50-mm
Air gap spacing between third glazing and fourth glazing, L_4	50-mm

The physical domain being analysed is the upper section of an FPSC, specifically from the absorber plate top to the glazing. This domain was chosen to focus on the temperature and the top heat loss occurring at the absorber plate across various configurations. It was assumed that the collector operates under steady-state conditions, and the effects of ambient temperature and solar irradiation were considered uniform across the surface. An emissivity of unity was assumed for the absorber plate ($\varepsilon_g = 1$) and the glazing ($\varepsilon_p = 1$) to simplify radiation analysis and ensure consistent comparison

across all glazing configurations. The transmittance of glass was determined using its refractive index, which was set to 1.5 to represent common glazing properties of FPSC. The ambient was assumed to have a constant convective heat transfer coefficient of 5 W m^{-2} K^{-1}, representing the convection in calm air. The Boussinesq approximation was applied for air in the air gap, assuming moderate temperature variations are within acceptable limits for natural convection modelling and faster convergence. The sides and bottom of the domain were assumed to be adiabatic so that heat can be lost only from the top surface of the glazing. The ambient temperature was assumed to be 303.15 K. These assumptions and considerations were made to isolate the influence of glazing on the top heat loss and absorber plate average temperature. The assumptions and constant parameters are tabulated in Table 3-2 below.

Table 3-2 Assumptions and constant parameters for the physical domains.

Assumptions and Constant Parameters	**Value**
System	Steady-state condition
Ambient temperature across the surface	Uniform
Solar irradiation across the surface	Uniform
Emissivity for the absorber plate and the glazing	Unity (equal to 1)
Refractive index of glass (transmittance)	1.5
Convective heat transfer coefficient of the ambient	Constant at 5 W m^{-2} K^{-1}
Buoyancy of air	Boussinesq approximation
Sides and bottom of the physical domain	Adiabatic
Ambient temperature	303.15 K

3.3 VALIDATION

To ensure the reliability of the simulation of this study, studies from Subiantoro & Ooi (2013) and Wang et al.'s (2017) are replicated and validated using Computational Fluid Dynamics (CFD) approach, following closely to their reported configuration and parameters. The Computational Fluid Dynamics (CFD) applications used is ANSYS Fluent software. The replication results closely matched the original finding (below 5 % in deviation), confirming the reliability of the methodologies employed. The validated results from these benchmark studies were then used as a reference to verify that the present model can accurately capture the key heat transfer mechanisms, particularly natural convection and radiation, under similar boundary conditions. This validation process also serves to assess whether the simulation performs as intended and is suitable for similar future applications involving on natural convection and radiation effects in thermal systems.

3.3.1 Subiantoro & Ooi (2013) Validation

Subiantoro & Ooi's (2013) study presents the analytical models that allow the prediction of heat loss for both single as top cover which enables analysis of a FPSC with narrow gap between the absorber and the top cover. The small gap in which it correlates with having low Rayleigh numbers is the main focus for Subiantoro and Ooi's (2013) study as Rayleigh number is used as a key parameter in modelling convective heat loss from the collector's top cover. Wang et al's (2017) study focuses on evaluating the impact of radiation modelling on temperature distribution by simulating natural convection in a cubical cavity at high Rayleigh numbers.

Subiantoro & Ooi's (2013) study focuses on comparing their new single-glazing model with the model proposed by Akhtar & Mullick, (1999), particularly in terms of

the top heat loss coefficient (U_t) and the glass cover temperature (T_g). They used both Akhtar and Mullick's (1991) analytical method and their own 2-D CFD model developed in ANSYS Fluent 13. The model simulates a single-glazing solar collector across various generalized Rayleigh numbers (Ra'), based on different gap spacings. The generalized Rayleigh numbers is defined as a modified form of the Rayleigh number (Ra) used in natural convection analysis when the surface is inclined at an angle β to the vertical and its equation is given by:

$$Ra' = Ra \cos \beta$$

where Ra is the Rayleigh number and β is the collector tilt angle.

Their 2-D rectangular model applied symmetrical side boundaries, mixed convection and radiation at the top surface to represent the glazing, and a constant temperature boundary at the bottom to represent the absorber plate as shown in Figure 3.3.

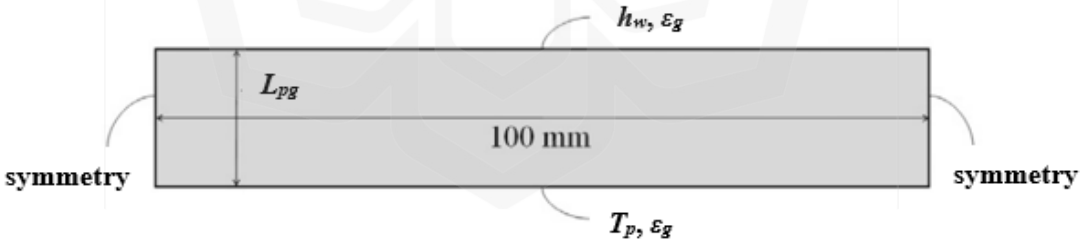

Figure 3.3 CFD model of single glazing FPSC from Subiantoro & Ooi, (2013).

The Surface-to-Surface (S2S) radiation model and ideal gas law for air density were used, with the PRESTO! scheme selected for pressure discretization method. Convergence was achieved when the energy and other residuals dropped below 10^{-7} and 10^{-4}, respectively. These conditions were later replicated and verified using ANSYS Fluent 22 R1. For verification, a 25 mm gap spacing from Subiantoro and Ooi's (2013)

study was used. Most ANSYS Fluent settings were retained as described in their study as shown in Table 3-1, with adjustments only made when required by the software. The boundary conditions matched those specified in Subiantoro and Ooi's (2013) 2-D model, which is included in Table 3.3.

Table 3-3 The boundary conditions and ANSYS Fluent settings of replicated 2-D model with 25 mm gap spacing from Subiantoro and Ooi's (2013) study.

Side Surfaces Boundary Condition	Adiabatic Boundaries
Top Surface Boundary Condition	Mixed Boundary of Convection and Radiation
Bottom Surface Boundary	Constant Temperature
Radiation Model	Surface To Surface (S2S) Model
Pressure Discretization Method	PRESTO! Scheme

These adjustments included the general, viscous, and radiation model settings. The setting of energy equation in ANSYS Fluent is enabled. For viscous model, the laminar model is used as Subiantoro and Ooi's (2013) did not specify which viscous model they used, and the value of *Ra'* for the 2-D model with air gap of 25-mm is low at 27000 as given by them. The radiation model of the Surface-to-Surface (S2S) model required the setup of view factor and cluster parameters in ANSYS Fluent.

Additionally, another modified version of the model was created and simulated by extending the 2-D simulation into 3-D for Subiantoro and Ooi's (2013) study, adding a 500-mm length dimension, resulting in a 25-mm × 100-mm × 500-mm domain. Again, most settings were retained unless prompted by ANSYS Fluent.

For 2-D simulation, both S2S and Discrete Ordinates (DO) radiation models are used, and the residual and energy convergence is achieved in less than 1000 iterations which indicates that the numerical solution has stabilized and is no longer changing significantly with further iteration. Figure 3.4 (a), (b) and (c) shows the comparison of the temperature contour of the replicated 2-D model (S2S and DO) and Subiantoro & Ooi's 2-D model. The comparison shows that temperature contour of both of the results is almost exactly similar to each other.

In this study, the boundary conditions, radiation model, pressure discretization method and the value of *Ra'* were selected from Subiantoro and Ooi's (2013) study itself to ensure that the simulation is accurately replicated. The boundary conditions define the temperature and heat flux at the absorber and glazing surfaces, establishing the driving potential for conduction, convection, and radiation within the collector. The radiation model governs how thermal radiation is exchanged between surfaces and through the glazing, directly affecting the absorber temperature and top heat loss. The pressure discretization method ensures numerical stability and accurate prediction of natural convection within the air gap, which strongly influences the convective component of heat loss.

The Rayleigh number, derived from the temperature difference, air gap height, and fluid properties, characterizes the convection regime (laminar or turbulent) and validates that natural convection is properly captured in the simulation. Lastly, the air gap is calculated from the chosen *Ra'* and its dimension controls the strength of radiative and convective coupling between the absorber and glazing layers. Together, these parameters and formulations establish the foundation for accurate temperature and heat loss predictions in both the validation and main simulation cases.

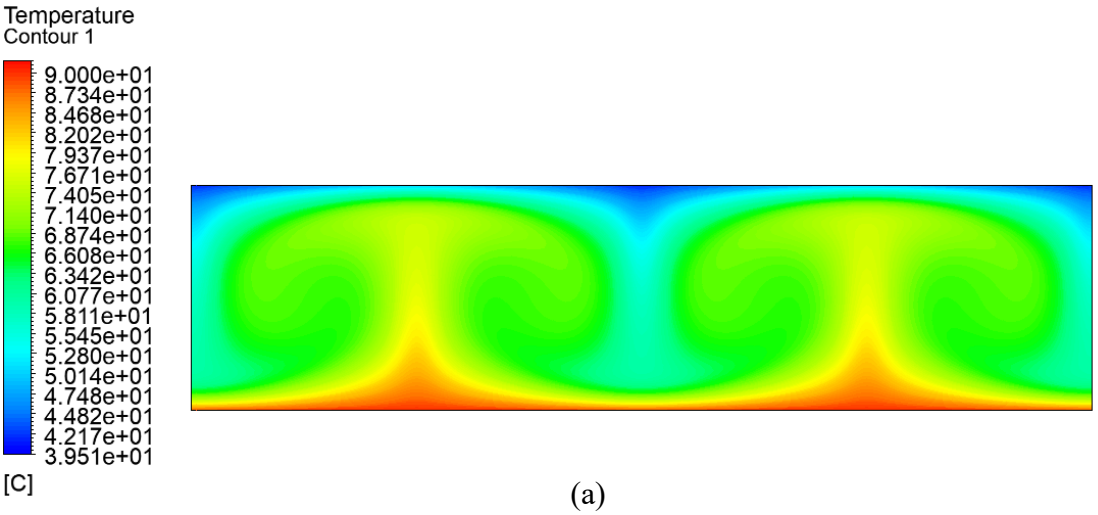

(a)

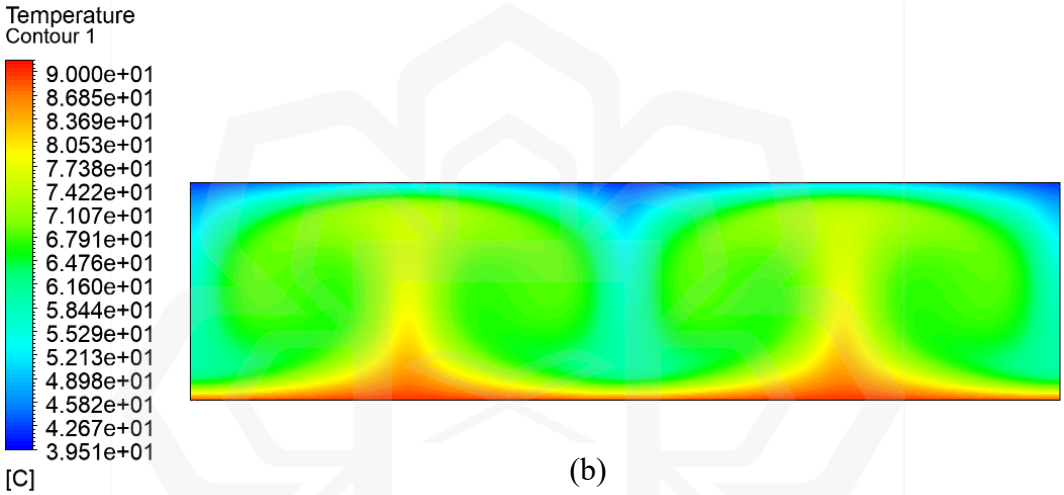

(b)

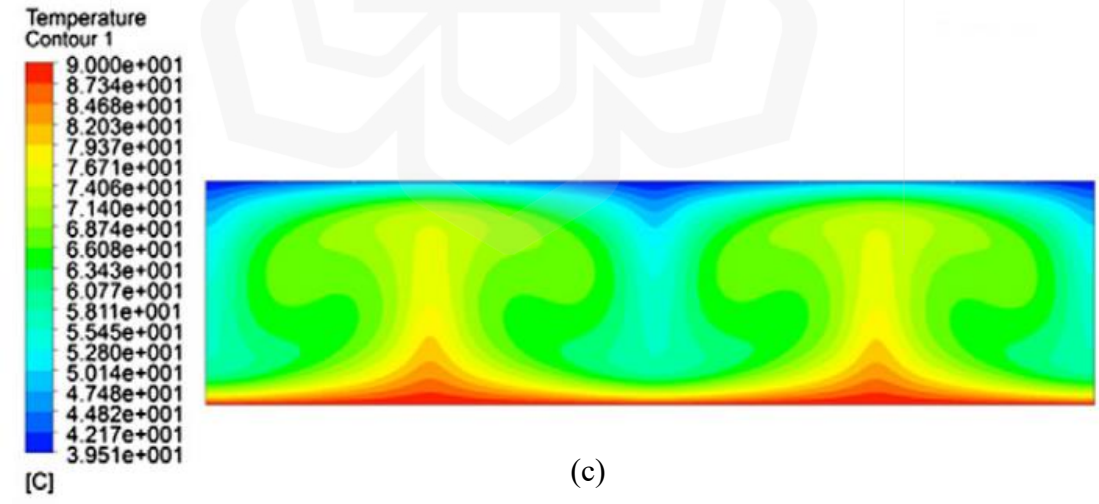

(c)

Figure 3.4 (a) The temperature contour of replicated 2-D model (S2S), (b) the temperature contour of replicated 2-D model (DO) and (c) the temperature contour of Subiantoro & Ooi's (2013) 2-D model.

For the replication of Subiantoro & Ooi's (2013) 2-D models, the adiabatic and mixed boundary conditions applied to the side wall and top surface, respectively, are adopted in this study to represent the insulation of the casing and glazing as well as simulating a natural convection in FPSC.

In the replicated 3-D model (S2S and DO radiation model), convergence was not achieved after 1000 iterations, as the residual stop dropping after 100 iterations and start to stall without going down or up significantly as more iterations goes. Performing more simulation until 3000 iterations also resulting in stalling of the residual. However, accuracy was verified through heat transfer and energy balance checks. The obtained values of the parameters compared for both the S2S and DO radiation models are similar to each other. The Nusselt number (*Nu*), used to assess heat transfer behaviour, was 10.3446 for the 2-D model and 9.9223 for the 3-D model, showing only a 4.08 % difference, indicating consistent thermal behaviour. Energy balance verification showed minimal imbalance: 1.35404×10^{-6} W for the 2-D model and 0.00691 W for the 3-D model, confirming accurate energy conservation as the value of net heat imbalance is very small. Additionally, the area-weighted average top surface temperatures were 319.32 K (2-D) and 318.36 K (3-D). The top surface temperature calculated for Subiantoro & Ooi's (2013) case was 317.80 K, so for 2-D model, its deviated by just 0.48 % and 1.76 % for 3-D, demonstrating strong agreement between both simulations.

Table 3-4 Comparison of results of current works 2D and 3D, and Subiantoro & Ooi (2013).

Parameter	**2-D Model**	**3-D Model**	**Subiantoro & Ooi's (2013) case**	**% Error / Deviation**
Nusselt Number (N_u)	10.3446	9.9223	-	4.08 %
Energy Imbalance (W)	1.3540413×10^{-6}	0.00691	-	–
Top Surface Temperature (K)	319.32	318.36	317.80	0.48 % (2-D) 1.76 % (3-D)

3.3.2 Wang et al. (2017) Validation

To validate further the 3-D model, the work of Wang et al. (2017) is used, since the residuals of the 3-D FPSC from the validation of Subiantoro & Ooi (2013) were stalled before reaching the convergence criteria. Wang et al. (2017) conducted a numerical study on natural convection within a cubical cavity with differentially heated side walls, using the Coupled Discrete Unified Gas-Kinetic Scheme (CDUGKS). This method, an enhanced version of DUGKS, was designed to simulate incompressible thermal flows at high Rayleigh numbers (up to 10^{10}), which require fine mesh near the walls to resolve thin boundary layers. The study demonstrated CDUGKS's ability to accurately capture temperature and velocity boundary layers near isothermal walls, outperforming traditional CFD solvers. It was noted that as the value of *Ra* increases with the increment of cubical height, boundary layers thin out and heat transfer shifts from conduction to convection.

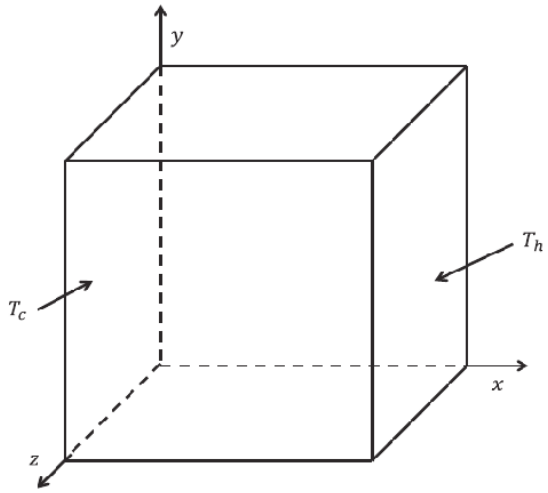

Figure 3.5 The schematic diagram of 3-D cubic model of Wang et al's (2017) study.

From Figure 3.5, the cubic cavity setup included a cold wall ($T = T_c$) on the left and a hot wall ($T = T_h$) on the right, with the remaining walls adiabatic and gravity acting in the y-direction. The box length was set to $H = 1$ and the Prandtl number to 0.71. Wang et al. validated their CDUGKS results by comparing them with experimental data from Mach-Zehnder interferometry technique from Krane & Jessee, (1983) and numerical results from a Finite Difference Navier-Stokes solver (Fusegi et al., 1991), confirming the accuracy of their model through close agreement in temperature and velocity profiles along the cavity's symmetry plane.

In order to replicate one of the result from Wang et al. (2017) in ANSYS Fluent software, some of the configuration from the paper need to be converted into fixed numerical value. The non-dimensional temperature of the cold wall, $T_c = 0$, and hot wall temperatures $T_h = 1$ need to be converted into numerical value in ANSYS Fluent software. Using the equation provided by Fusegi et al. (1991) and assuming that the dimensional value cold wall of T^*_c is 300 K, the value of T^*_h is obtained. The Rayleigh number equation is used to calculate the dimensional value of H since Wang et al. (2017) only list it as non-dimensional value of $H = 1$. The chosen Rayleigh number is

$Ra = 10^5$. The following equations are used to obtain the value of H (Fusegi et al., 1991; Wang et al., 2017).

At $x = 0$,

$$T_c = \frac{(2 - \delta)}{2} \tag{1}$$

At $x = 1$,

$$T_h = \frac{(2 + \delta)}{2} \tag{2}$$

where T_c is the non-dimensional temperature of the cold wall, T_h is the non-dimensional temperature of the hot wall and δ is the overheat ratio.

Based on the assumption that T^*_c is 300 K, the value of the dimensional film temperature of the wall, T^*_o, and the value of the dimensional temperature of hot wall, T^*_h can be calculated using the given equations:

$$T_o^* = \frac{T_c^*}{T_c} \tag{3}$$

$$T_h^* = \frac{T_h}{T_o^*} \tag{4}$$

By using the equation for Rayleigh number, the dimensional value of the cavity of the cube model, H (m) can be obtained (Cengel & Ghajar, 2014; Wang et al., 2017):

$$R_a = \frac{g \times \beta \times \Delta T \times H^3 \times P_r}{v^2} \tag{5}$$

$$\beta = \frac{1}{T_o^*} \tag{6}$$

$$\Delta T = T_h^* - T_c^* \quad (7)$$

where g is the gravitational acceleration (m s^{-2}), β is the volume expansion coefficient of an ideal gas (K^{-1}), ΔT is the temperature difference between hot and cold wall (K), P_r is the Prandtl number (the value is 0.71), and v is the kinematic viscosity of air at film temperature (m^2 s^{-1}).

The obtained dimensional value of H is approximately 35-mm, making the dimension of cube model in ANSYS Fluent as 35-mm × 35-mm × 35-mm. These dimensional value help to realize the replication of the Wang et al.'s result in ANSYS Fluent. For the mesh distribution of the model in ANSYS Fluent, it is distributed non-uniformly, with a gradual refinement near the walls to more accurately capture boundary layer effects using the subdivision of meshes features as shown in Figure 3.6.

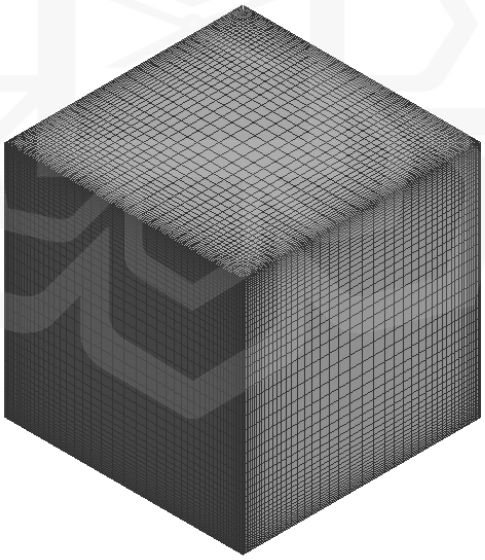

Figure 3.6 The mesh of replicated model from Wang et al. (2017).

The replicated model based on the results from Wang et al.'s (2017) study consists of three different radiation models; one without radiation model which is ANSYS (No Radiation), another using the S2S model (S2S Model) and DO radiation

model (D) Model). For the model without radiation model, the convergence is achieved after 70 iterations and for S2S and DO model, it took 76 iterations. Figure 3.7 and Figure 3.8 shows the temperature distribution on the symmetry plane of $z = 0.5$ for $Ra = 10^5$ for x versus T/T_0 and y vs T/T_o, respectively. Both results from replicated model is compared to the result from Fusegi et al. (1991), Krane & Jessee (1983), and Wang et al. (2017).

Figure 3.7 shows the comparison of temperature distribution (T/T_o) along the x-direction for different models and experimental data. The results from ANSYS for both of no radiation model, S2S and DO model closely match the experimental data from Wang et al. (2017), Fusegi et al. (1991), and Krane & Jesse (1983), demonstrating good agreement. The temperature remains relatively uniform in the middle region ($0.2 < x < 0.8$) but exhibits a noticeable rise near the boundaries. This indicates that the replicated models effectively capture the thermal behaviour, with only slight deviations between numerical and experimental results.

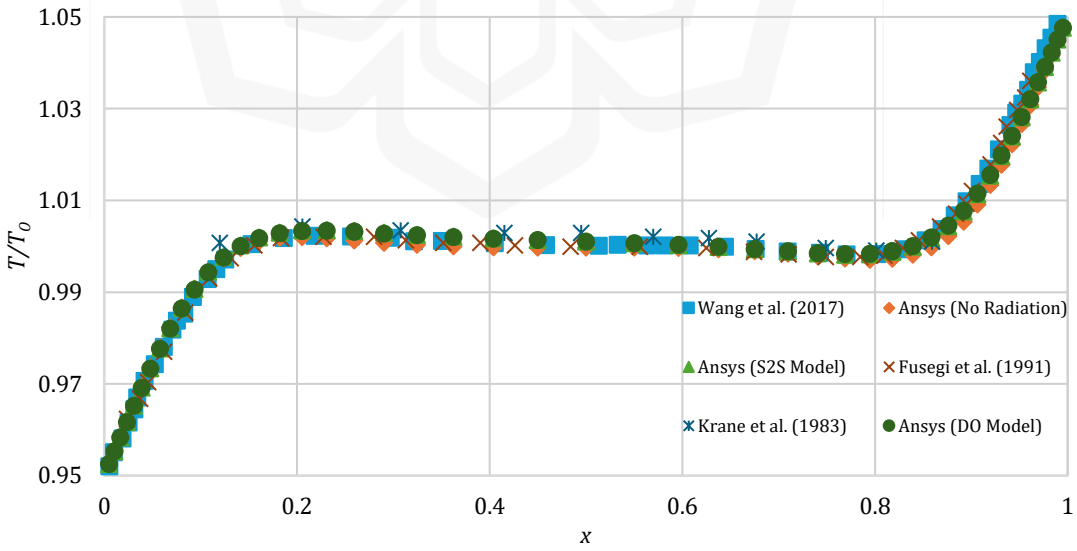

Figure 3.7 Comparison of current model using ANSYS Fluent on the temperature distribution on the symmetry plane of $z = 0.5$ (x vs T/T_o) against Wang et al. (2017), Fusegi et al. (1991) and Krane & Jessee, (1983).

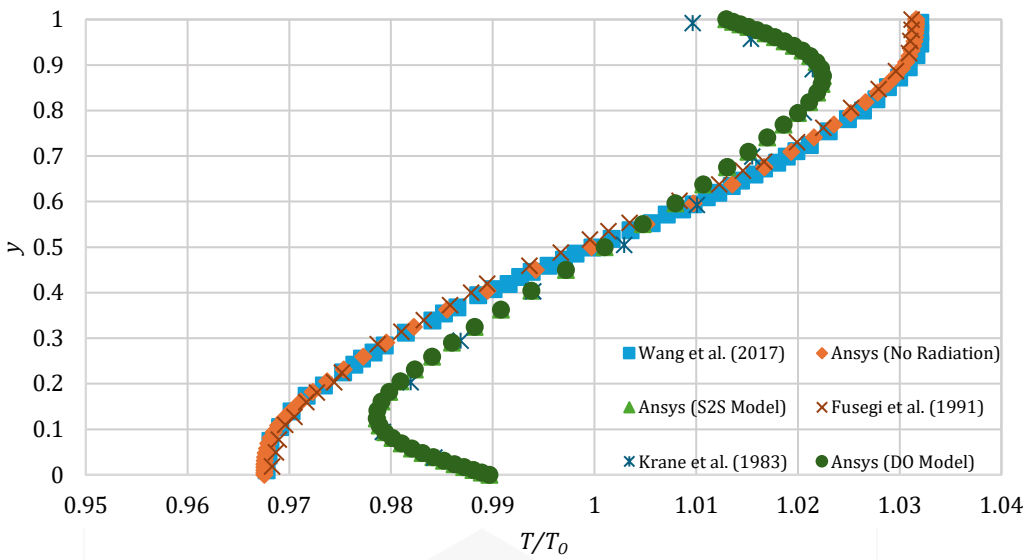

Figure 3.8 Comparison of current model using ANSYS Fluent on the temperature distribution on the symmetry plane of $z = 0.5$ (y vs T/T_o) against Wang et al. (2017), Fusegi et al. (1991) and Krane & Jessee, (1983).

Figure 3.8 showed the comparison of the temperature distribution (T/T_o) along the y-direction between different models and experimental data taken from Wang et al. (2017). The results from the replicated model with no radiation model closely match, with below 2 % of difference when compared with the data from Wang et al. (2017) and Fusegi et al. (1991), indicating good agreement. However, the replicated model using the S2S and DO radiation model deviates significantly from the numerical studies of Wang et al. (2017) and Fusegi et al. (1991), but closely follows the experimental data from Krane & Jessee, (1983), suggesting that the S2S and DO radiation model predicts different thermal behaviour compared to numerical results, yet aligns more accurately with experimental data. This discrepancy highlights the ability of S2S radiation modelling in simulating thermal radiation.

The replication of Subiantoro & Ooi's (2013) and Wang et al.'s (2017) studies using ANSYS Fluent successfully verified key thermal behaviors in single-glazing flat plate solar collectors and natural convection in a cubical cavity. The 2-D and 3-D

collector models for Subiantoro & Ooi's (2013) study showed good agreement with the original data, with minimal discrepancies in Nusselt number (4.26 %) and top surface temperature (0.3 %), and acceptable energy imbalances, confirming numerical accuracy. Although the 3-D model did not converge after 1000 iterations, the results remained reliable. In order to further validate thermal radiation for 3-D case, Wang et al. (2017) work is replicated, and a good agreement was observed with previous numerical and experimental results. By including the Surface-to-Surface (S2S) radiation model, the model showed better agreement with the experimental data which indicate its capability to capture a more realistic result. These findings highlight ANSYS Fluent's capability in thermal simulations and highlight the critical role of boundary and radiation modelling choices in achieving accurate results.

3.4 FPSC MODEL DEVELOPMENT

Based on the foundation from the validation process, the 3-D models of this simulation study are developed tailored for this specific research objectives. The ANSYS software is used to develop the simplified 3-D models. Each configuration of FPSC are developed in ANSYS Spaceclaim and ANSYS Meshing. In ANSYS Spaceclaim, the simplified models of FPSC are created for each configuration, the number of glazing layer and glazing layer thickness. A total of eight simplified models of the FPSC have been developed for this study. Four models were developed for FPSCs with 1-, 2-, 3-, and 4-glazing layers as shown in Figure 3.9. Then additional four models were created to study the effect of different glazing thicknesses, ranging from 2-mm, 3-mm, 4-mm, and 5-mm, based on a selected number of glazing layers.

In order to study the effect of the number of glazing layer configuration on the FPSC, the configuration of 1-, 2-, 3-, and 4-glazing layers are developed as shown in Figure 3.9. The models have the same dimensions for the width and length, which is 500-mm × 300-mm, resulting in 0.15-m^2 of absorber plate area. The gap distance between the absorber plate, glazing and the subsequent glazing layer is maintained at 50-mm. For the number of glazing layer study, the glazing thickness is set at 4-mm. The thickness of the insulator and absorber plate is 20-mm and 1-mm, respectively.

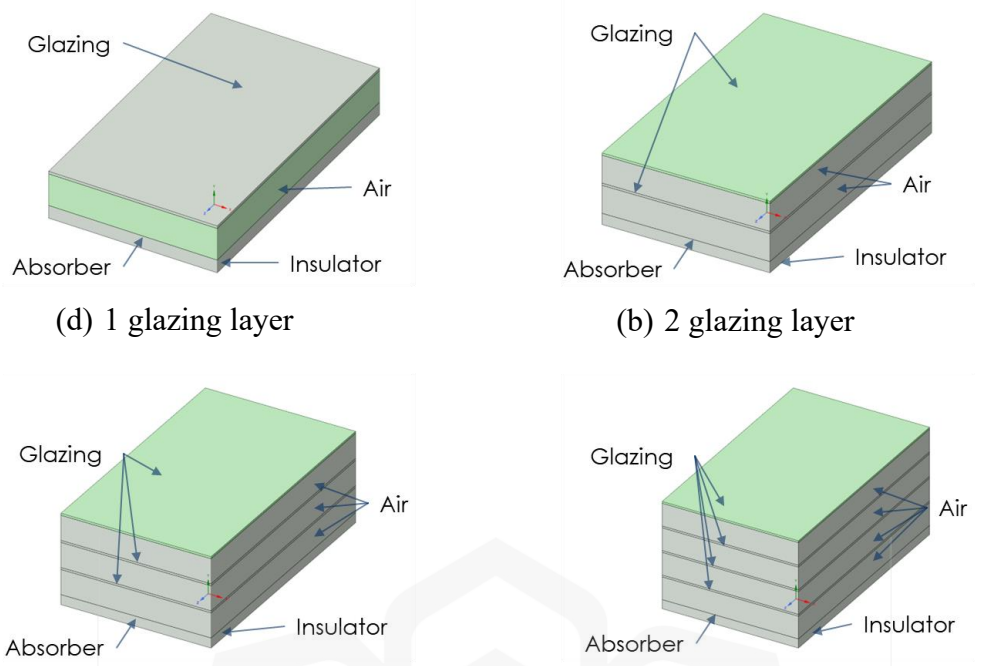

Figure 3.9 The simplified 3-D models of FPSC for the configuration of number of glazing layer.

In ANSYS Meshing, the mesh is created using the number of divisions function and bias type of smaller division near the edge of the model for to create non-unifom and finer mesh near wall boundary of the model, as shown in Figure 3.10, for better prediction of heat transfer and fluid flow behaviour. The number of elements of mesh present in all of the developed FPSC model range from 1.75×10^6 for single glazing model up to 7.75×10^6 for 4 glazing layer model which enough to reach residual and energy convergence in the simulation. Figure 3.10 shows the non-uniform and finer mesh near wall boundaries of the models.

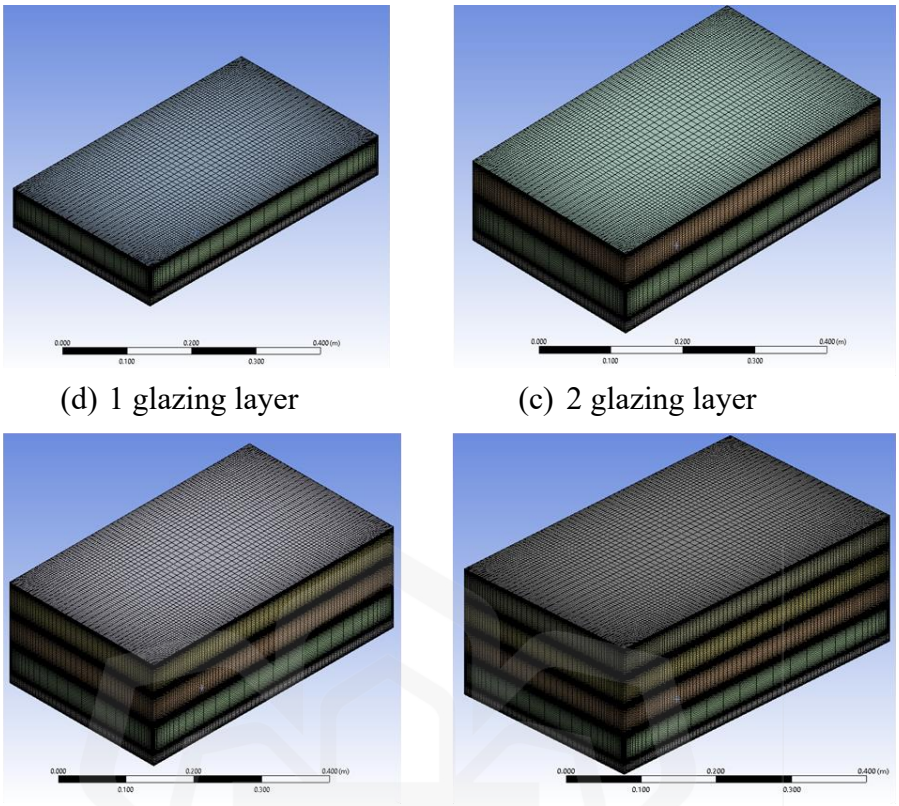

(d) 1 glazing layer (c) 2 glazing layer

(b) 3 glazing layer (a) 4 glazing layer

Figure 3.10 The non-uniform and finer mesh near wall boundaries of the models.

In ANSYS Fluent software, the energy equation is enabled. For viscous model, the standard k-epsilon model is selected due to its acceptable accuracy for heat transfer and flow simulations. DO radiation model is selected for radiation model as it enables the definition of semi-transparent interior and exterior walls in ANSYS Fluent which is useful to specify the absorber and glazing properties. The solar load model used is solar irradiation with the longitude and latitude of Kuala Lumpur, Malaysia at 1 p.m. time. The sun direction vector, direct solar irradiation and diffuse solar irradiation is calculated by the software, based on the global position and time given. The calculated value of direct irradiation is 874 W m^{-2} and the diffuse irradiation is 102 W m^{-2}. These values of irradiations accounts for the position of the Sun and the scattered sunlight due to atmospheric effect such as partial cloud covering. Hence, these irradiation values are considered representative of realistic operating conditions for FPSC exposed to direct

sunlight with atmospheric scattering.. Both irradiations are used for the simulation of the FPSC receiving total solar radiation. For spatial discretization, the second order upwind scheme is used as it provides more accurate results although at the cost of slower convergence. Table 3-5 shows the setup for the simulation. The material and its properties of the components in the FPSC model are shown in the table 3-6.

Table 3-5 The setting of the simulation.

Solver type	Pressure-Based
Time	Steady
Gravitational Acceleration	-9.81 at Y-direction
Energy	On
Viscous Model	Standard k-epsilon
Radiation Model	Discrete Ordinates (DO)
Solar Load Model	Solar Irradiation

Table 3-6 The material and its properties of the components in the FPSC model.

Component	Absorber	Casing	Glazing	Insulator	Air Gap
Material	Copper	Aluminium	Glass	Polyurethane Foam	Air
Density (kg m^{-3})	8933	2702	2800	24	1.1644
Specific heat capacity, C_p (J kg^{-1} K^{-1})	385	903	750	1200	1006.43
Thermal conductivity, k (W m^{-1} K^{-1})	401	230	0.7	0.023	0.0242

The wall boundary condition for absorber is set to mixed (convection and radiation) with the surrounding temperature is set at 303.15 K, heat transfer coefficient of stagnant air at 5 W m^{-2} K^{-1}, and emissivity of 1 as well as opaque. The casing or the side wall of the model and the bottom of the insulator is adiabatic and opaque to simulate the insulation taking place inside FPSC. The bottom and top surface glazing has the same thermal boundary conditions as absorber; however, their radiation boundary is set as semi-transparent to allow the radiation to pass through. The transmittance of glass was determined using its refractive index, which was set to 1.5 to represent common glazing properties of FPSC.

The contact region of absorber and glazing with air domain is set to coupled, to allow the heat transfer between them. The Boussinesq approximation was applied for air in the air gap, assuming moderate temperature variations are within acceptable limits for natural convection modelling and for faster convergence. The simulation is considered as converged when residuals of the energy, do-intensity and all other parameters are below the default setting criteria, which are 10^{-6}, 10^{-6} and 10^{-3}, respectively.

For the study of the glazing thickness, the selected model will be modified by adjusting the thickness glazing, where four new models will be developed with varying thickness of 2-mm to 5-mm, as mentioned earlier. The selection of the model from the study of number of glazing layers for further investigation of glazing thickness will be discussed in Chapter 4.

Table 3-7 The glazing thickness for each configuration for thickness study.

Geometrical Parameters	Value
Glazing thickness configuration, L_g	2-mm to 5-mm
Absorber plate thickness, L_p	20-mm
Air gap spacing between absorber plate and first glazing, L_1	50-mm
Air gap spacing between first glazing and second glazing, L_2	50-mm
Air gap spacing between second glazing and third glazing, L_3	50-mm
Air gap spacing between third glazing and fourth glazing, L_4	50-mm

3.5 TOP HEAT LOSS COEFFICIENT (U_t) AND RATE OF USEFUL HEAT (Q_u)

This section focuses on the parameters and formula that will be used for the calculations and analysis of this study, which mainly include the temperature of absorber plate and each glazing surfaces, top heat loss coefficient (U_t) and useful heat gain (Q_u). By obtaining directly the numerical results of each temperature of absorber plate and each glazing surfaces from ANSYS Fluent simulation and the designated parameters mentioned in Chapter 3.2 and Chapter 3.3 (ambient temperature and the convective heat transfer coefficient of ambient and stagnant air), the value of convective and radiative heat transfer coefficient between plate and first glazing and subsequent glazing layers can be determined as discussed later in this chapter. These calculated coefficients are then used to evaluate the top heat loss coefficient for each glazing number configuration and thickness, following the equations presented in the later sections also in this chapter.

Majority of heat loss of a solar collector occur at the top through the glazing which is called top heat loss (Akhtar & Mullick, 1999). When compared to bottom and side heat loss, top heat loss is more significant, so reducing the top heat loss coefficient, U_t is important because it directly lowers the overall loss coefficient, U_L, thereby

increasing the useful energy gain of FPSC. The U_t is determined by accounting for both convective and radiative losses from the absorber plate in the upward direction. It is also can be obtained by considering the convective and radiative heat transfer coefficients within the FPSC. The total thermal heat loss, U_L can be defined as:

$$U_L = U_t + U_b + U_s \tag{8}$$

where U_b is the bottom heat loss coefficient (W m^{-2} K^{-1}) and U_s is the side heat loss coefficient (W m^{-2} K^{-1})

Since the U_b and U_s is assumed to be negligible, they were excluded from this study, so:

$$U_L = U_t \tag{9}$$

For single glazed FPSC, the U_t can be defined as (Samdarshi & Mullick, 1988):

$$U_t = \left[U_{pg1}^{-1} + U_{g1a}^{-1} + \frac{L_g}{k_g}\right]^{-1} \tag{10}$$

where U_{pg1} is the overall heat transfer coefficient between absorber plate and first glazing (W m^{-2} K^{-1}), U_{g1a} is the overall heat transfer coefficient between first glazing and ambient (W m^{-2} K^{-1}), L_g is the thickness of glazing (m) and k_g is the thermal conductivity of glazing (W m^{-1} K^{-1}).

The overall heat transfer coefficient between absorber plate and first glazing, and between first glazing and ambient air can be defined as $U_{pg1} = \left(h_{cpg1} + h_{rpg1}\right)$ and $U_{g1a} = (h_w + h_{rg1a})$, therefore the top heat loss coefficient, U_t of a single glazed FPSC can be expressed as:

$$U_t = \left[\left(h_{cpg1} + h_{rpg1}\right)^{-1} + \left(h_w + h_{rg1a}\right)^{-1} + \frac{L_g}{k_g}\right]^{-1} \quad (11)$$

where h_{cpg1} is the convective heat transfer coefficient between plate and first glazing (W m^{-2} K^{-1}), h_{rpg1} is the radiative heat transfer coefficient between plate and first glazing (W m^{-2} K^{-1}), h_w is the wind heat transfer coefficient (W m^{-2} K^{-1}) and h_{rg1a} is radiative heat transfer coefficient between first glazing and ambient air (W m^{-2} K^{-1}).

For double glazed FPSC, the top heat loss coefficient, U_t can be defined as (Mullick, 1991):

$$U_t = \left[\left(h_{cpg1} + h_{rpg1}\right)^{-1} + \left(h_{cg1g2} + h_{rg1g2}\right)^{-1} + \left(h_w + h_{rg2a}\right)^{-1} + \frac{2L_g}{k_g}\right]^{-1} \quad (12)$$

where h_{cg1g2} is the convective heat transfer coefficient between first glazing and second glazing (W m^{-2} K^{-1}), h_{rg1g2} is the radiative heat transfer coefficient first glazing and second glazing (W m^{-2} K^{-1}), and h_{rg2a} is the radiative heat transfer coefficient between second glazing and ambient air (W m^{-2} K^{-1}).

To obtain the value of h_{cpg1}, h_{rpg1}, h_{cg1g2}, h_{rg1g2} and h_{rg2a}, following equations can be used (Bisen et al., 2011):

$$h_{cpg1} = \frac{K_1 \times N_{u1}}{L_1}, \quad (13)$$

$$h_{rpg1} = \left\{\frac{\sigma}{\frac{L_1}{\varepsilon_p} + \frac{1}{\varepsilon_g} - 1}\right\}\left(T_p^2 + T_{g1}^2\right)\left(T_p + T_{g1}\right), \quad (14)$$

$$h_{cg1g2} = \frac{K_2 \times N_{u2}}{L_2}, \tag{15}$$

$$h_{rg1g2} = \frac{\sigma}{\left\{\frac{2}{\varepsilon_g} - 1\right\}}\left(T_{g1}^2 + T_{g2}^2\right)\left(T_{g1} + T_{g2}\right), \tag{16}$$

$$h_{rg2a} = \sigma \cdot \varepsilon_g \frac{\left(T_{g2}^4 - T_{sky}^4\right)}{T_{g2} - T_a}, \tag{17}$$

where T_p is the absorber plate temperature (K), T_a is the ambient temperature (K), T_{sky} is the sky temperature (K), ε_g is the absorber plate emissivity, ε_p is the glazing emissivity, L_1 is the spacing between absorber plate and first glazing (m) , L_2 is the spacing between first glazing and second glazing (m), and K is the thermal conductivity of air (W m^{-1} K^{-1}).

The T_{sky} is calculated using the equation from Swinbank, (1963):

$$T_{sky} = 0.0552 \times T_a^{1.5}$$

The value of N_u can be calculated using these equations that depends on the obtained value of R_{a1} (Buchberg et al., 1976):

If $R_{a1} < 1708$, then $N_{u1} = 1,$ (18)

If $R_{a1} > 1708$ and $R_{a1} < 5900$, then,

$$N_{u1} = 1 + 1.446\left(1 - \frac{1708}{R_{a1}}\right). \tag{19}$$

If $R_{a1} > 5900$ and $R_{a1} < 9.23 \times 10^4$, then,

$$N_{u1} = 0.229 \times R_{a1}^{0.252}. \tag{20}$$

If $R_{a1} < 9.23 \times 10^4$ and $R_{a1} < 10^6$, then,

$$N_{u1} = 0.157 \times R_{a1}^{0.285}. \quad (21)$$

where K_1 is the thermal conductivity of air, evaluated at the arithmetic mean surface temperature.

The value of R_a can be evaluated by using this equation:

$$R_{a1} = \frac{9.8 \cdot (T_p - T_{g1})(L_1)^3(P_{r1})}{V_1^2\left(\frac{T_p + T_{g1}}{2}\right)} \quad (22)$$

where T_p is the absorber plate temperature, T_{g1} is the temperature of first glazing (K), L_1 is the gap spacing between the absorber plate and first glazing, P_{r1} is the Prandtl number of air, evaluated at the arithmetic mean surface temperature, V_1 is the kinematic viscosity of air, evaluated at the arithmetic mean surface temperature,

The following air properties correlation can be used to calculate R_{a1} (Bisen et al., 2011):

$$K_1 = -3 \times 10^{-8}\, T_m^2 + 10^{-4} T_m - 4 \times 10^{-5} \quad (23)$$

$$V_1 = -(9 \times 10^{-5} T_m^2 + 0.04 T_m - 4.17) \times 10^{-6} \quad (24)$$

$$P_{r1} = +1.057 - 0.06 log T_m \quad (25)$$

The arithmetic mean of the corresponding surface temperature (T_m) based on this equation:

$$T_m = \frac{T_p + T_g}{2} \quad (26)$$

The earlier equations apply to the layer between the absorber and the first glazing, and similar equations are used for the subsequent layers, such as between the first and second glazing, as well as for the third and fourth glazing layers. So, for the layer between the absorber and first glazing, the T_{m1} is calculated, then for the layer between the first and second glazing, T_{m2} is calculated and so on.

So, the top heat loss coefficient, U_t for FPSC with 3 glazing layers can be defined as:

$$U_t = \left[\left(h_{cpg1} + h_{rpg1}\right)^{-1} + \left(h_{cg1g2} + h_{rg1g2}\right)^{-1} + \left(h_{cg2g3} + h_{rg2g3}\right)^{-1} + \left(h_w + h_{rg3a}\right)^{-1} + \frac{3L_g}{k_g} \right]^{-1} \quad (27)$$

where h_{cg2g3} is the convective heat transfer coefficient between second glazing and third glazing (W m^{-2} K^{-1}), h_{rg2g3} is the radiative heat transfer coefficient second glazing and third glazing (W m^{-2} K^{-1}), and h_{rg3a} is the radiative heat transfer coefficient between third glazing and ambient air (W m^{-2} K^{-1}).

And for FPSC with 4 glazing layers:

$$U_t = \left[\left(h_{cpg1} + h_{rpg1}\right)^{-1} + \left(h_{cg1g2} + h_{rg1g2}\right)^{-1} + \left(h_{cg2g3} + h_{rg2g3}\right)^{-1} + \left(h_{cg3g4} + h_{rg3g4}\right)^{-1} + \left(h_w + h_{rg4a}\right)^{-1} + \frac{4L_g}{k_g} \right]^{-1} \quad (28)$$

where h_{cg3g4} is the convective heat transfer coefficient between third glazing and fourth glazing (W m^{-2} K^{-1}), h_{rg3g4} is the radiative heat transfer coefficient third glazing and fourth glazing (W m^{-2} K^{-1}), and h_{rg4a} is the radiative heat transfer coefficient between fourth glazing and ambient air (W m^{-2} K^{-1}).

In addition, the rate of useful energy extracted, Q_u is calculated as the difference between the rate of incoming solar radiation, Q_i and the rate of heat loss, Q_o, which also factors in the temperature of collector, T_p and ambient temperature, T_a is (Struckmann, 2008),

$$Q_o = U_L A(T_p - T_a) \tag{29}$$

$$Q_u = Q_i - Q_o = I\tau\alpha \cdot A - U_L A(T_p - T_a) \tag{30}$$

where I is the intensity of solar radiation W m^{-2}, $\tau\alpha$ is the product of the rate of transmission of the glazing and the absorption rate of the absorber, and A is the absorber surface area (m^2). The value of I can be obtained from the solar load calculator in ANSYS Fluent software. The value of $\tau\alpha$ is set to 0.9 in order to closely replicate the real-world performance of the glazing and absorber plate in a FPSC.

The value of the T_p, T_{g1}, T_{g2}, T_{g3} and T_{g4} are obtained in the ANSYS Fluent software using the surface integral report function of area-weighted average. The value surface incident radiation, in W also was obtained, using the same report function. The calculation of U_t, Q_o, Q_u and related equations is done using the Microsoft Excel. In Microsoft Excel, the value of T_p, T_{g1}, T_{g2}, T_{g3} and T_{g4} is inserted into the temperature reading table. The basic Excel built-in functions and range references are used for arithmetic operation (addition, subtraction, multiplication and division), in order to obtain the value of T_m, K, V, P_r, R_a, N_u, h_c, h_r, U_t, Q_o and Q_u for each layers using the provided equations in this section.

3.6 SUMMARY

This chapter discusses and elaborates on the methodology used to achieve the objectives of this study, which involves simulation using ANSYS Fluent software and calculation of U_t, Q_o and Q_u. The simplified 3-D CFD models of FPSC are developed, and their simulation settings and parameters are described in detail. The models allow the study to focus on the configuration of the number of glazing layers and glazing thickness, with the former being investigated first, followed by the investigation of the latter.

CHAPTER FOUR

RESULT AND DISCUSSION

This chapter presents and discusses the key findings of this study, focusing on the influence of number of glazing layers and glaizng thickness of FPSC. Chapter 4.1 examines the relationship between the number of glazing layers and their influence on U_t, the average temperature of absorber plate and each glazing layers (T_p, T_{g1}, T_{g2}, T_{g3} and T_{g4}), trend of the temperature difference of each layer, the distribution of surface incident radiation and useful heat gain. Subsequently, Chapter 4.2 explores the effects of glazing thickness on these same performance parameters to identify the optimal configuration that enhances heat retention while maintaining efficient solar energy absorption. Overall, this chapter aims to interpret the observed trends in relation to the underlying heat transfer mechanisms and validate how glazing configuration influences the collector's overall thermal efficiency.

4.1 NUMBER OF GLAZING LAYERS

The top heat loss is quantified by the overall top heat loss coefficient, U_t, which represents the combined effects of convective and radiative heat transfer through the glazing system as expressed in equations (11), (12), (27) and (28). For the current steady-state heat transfer with adiabatic conditions at the side walls and bottom wall, a lower U_t corresponds to reduced heat loss through convection and radiation from absorber plate to top glazing; thus, a higher absorber temperature was expected. Table 4-1 and Figure 4.1 show the obtained U_t, based on the calculation done in Microsoft Excel as stated in Chapter 3.4.

Table 4-1 The obtained U_t for each number of glazing layer configuration.

Configurations	Top Heat Loss Coefficients, U_t (W m^{-2} K^{-1})
1 Glazing	6.80
2 Glazing	4.33
3 Glazing	3.19
4 Glazing	2.52

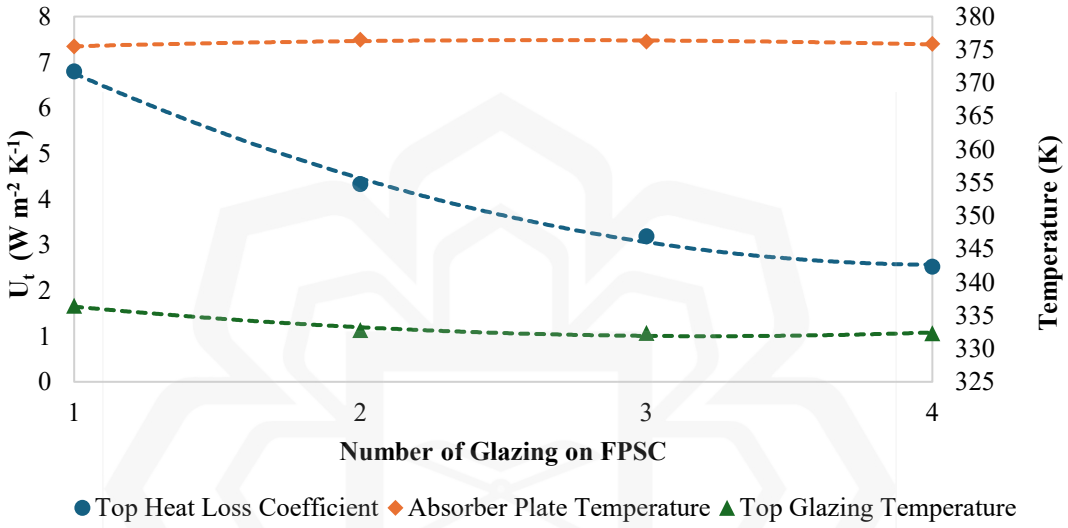

Figure 4.1 The obtained value of top heat loss coefficient, U_t.

Table 4-2 The average of temperature of plate absorber, T_p and temperature of each glazing layers.

Configurations	Average Absorber Plate Temp, T_p (K)	Average First Glazing Temp, T_{g1} (K)	Average Second Glazing Temp, T_{g2} (K)	Average Third Glazing Temp, T_{g3} (K)	Average Fourth Glazing Temp, T_{g4} (K)
1 Glazing	375.46	336.46	-	-	-
2 Glazing	376.48	358.03	332.77	-	-
3 Glazing	376.22	366.76	356.11	332.36	-
4 Glazing	375.87	370.74	365.45	355.81	332.28

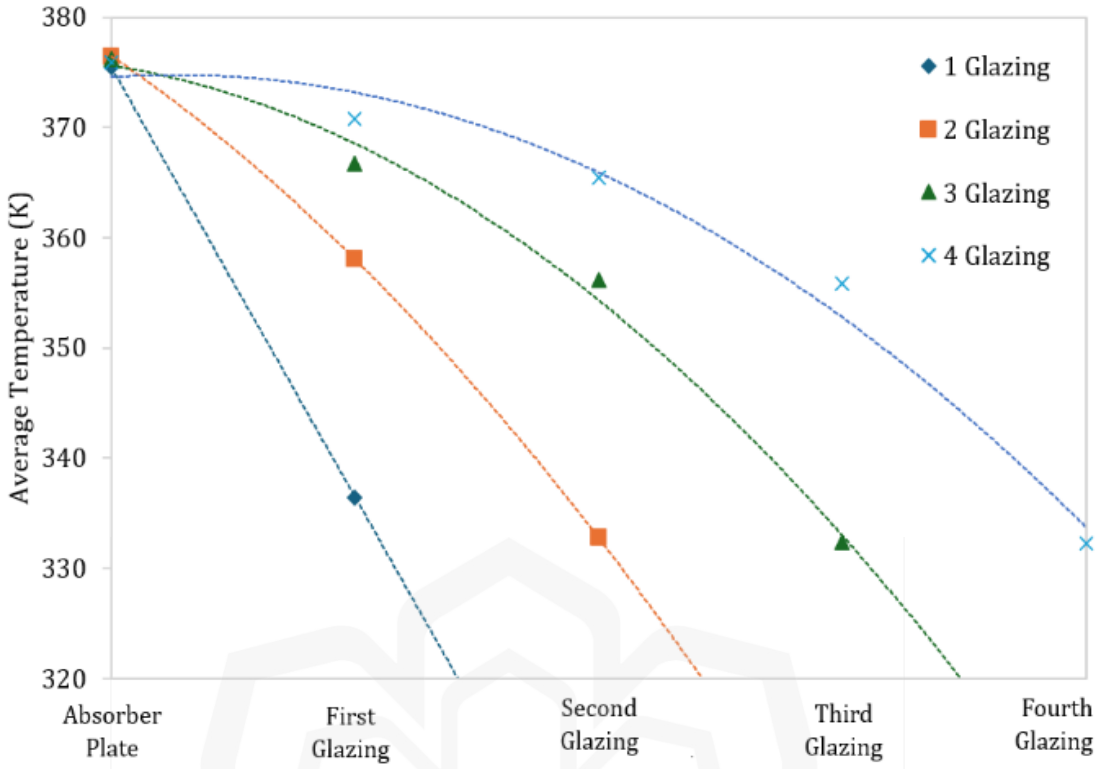

Figure 4.2 The average temperature of plate absorber, T_p and temperature of each glazing layers (T_{g1}, T_{g2}...).

Table 4-2 and Figure 4.2 show the obtained average of temperature of plate absorber, T_p and temperature of each glazing layers and its trend for the study of number of glazing layers on FPSC. The first glazing layer, T_{g1}, refers to the glazing layer at the bottom, which is the nearest to the absorber plate, followed by subsequent glazing layers from the bottom to the top (T_{g2}, T_{g3}…).

From Table 4-1 and Figure 4.1, the U_t was found to decrease with the addition of glazing layers. The rate of decrease of U_t between each glazing configuration is shown in Table 4-3. For instance, the U_t for a single glazing layer is 6.55 W m^{-2} K^{-1}, which drops significantly to 4.33 W m^{-2} K^{-1} for two layers, a 36.28 % reduction. Further additional glazing layer yields smaller incremental reductions, 26.44 % from two to three glazing, at 3.25 W m^{-2} K^{-1}, and only 20.80 % from three to four layers, at 2.62 W

m^{-2} K^{-1}. This trend aligns with the assumption that U_t will decrease as more glazing layers are added. However, the rate of decline also starts to slow down, suggesting that the effect of decreasing U_t starts to diminish with increasing glazing layer. The rate of changes of U_t is important to understand because it provides better understanding that can lead to a more efficient FPSC design, in term of performance and cost. By considering this rate, the optimal number of glazing layers required can be determined as well as the materials needed, thereby preventing excessive design and budget allocations.

Table 4-3 Comparison of U_t across each number of glazing layers configurations.

Configurations	**Rate of change of U_t (%)**
1-glazing to 2-glazing	36.28
2-glazing to 3-glazing	26.44
3-glazing to 4-glazing	20.80

Based on the equation of U_t, adding more glazing creates more resistance, mainly in terms of h_c and h_r as shown in the extension of the equations (11), (12), (27) and (28) with the calculation performed in Excel. Since these resistances are added in series, the total resistance becomes greater, and consequently, the inverse of the total resistance, which is the U_t will decrease.

In this numerical investigation, FPSC was modelled under steady-state conditions with a constant solar input and adiabatic side and bottom surfaces. The absorber plate temperature, T_p was utilised as an indirect indicator of top heat loss, hence overall collector performance. With controlled boundary conditions, with a constant solar input and adiabatic side and bottom surfaces, the absorber reached a steady-state temperature determined by the balance between absorbed solar energy and heat lost through the top surface via glazing. Under these conditions, A higher T_p

implies reduced top heat loss, while a lower T_p indicates increased heat loss through the glazing layers, as shown in Figure 4.2. This approach is consistent with established research practices in which absorber temperature is the performance metric when heat losses are eliminated (Kalougirou, 2004).

It is acknowledged that optical losses, reflection and absorption in the glazing layers can influence the overall energy balance. In this study, those optical effects were either explicitly modelled or assumed constant across all configurations, ensuring that any observed changes in absorber temperature are attributed primarily to differences in convective and radiative losses due to the number of glazing layers. The variations in thermal conductivity and specific heat resulting from changes of number of glazing layers and thickness are assumed to have a negligible influence on the collector's overall thermal performance.

The thermal conductivity and specific heat of the glazing were kept constant for all configurations, and this assumption is considered acceptable for the purpose of the present analysis. Under controlled boundary conditions, with the bottom and side walls set as adiabatic, only heat loss through the top surface occurs. Therefore, changes in absorber temperature reflect variations in top heat loss due to different glazing configurations. Table 4-2 and Figure 4.2 shows the obtained average temperature of the plate absorber, T_p, and the temperature of each glazing layer, along with the trend for studying the number of glazing layers on the FPSC as measured in ANSYS Fluent.

Based on the Table 4-2 and Figure 4.2, a non linear trend in T_p can be observed as glazing layer increases 1-glazing configuration yields 375.46 K, 2-glazing peak at 376.48 K, 3-glazing plunge to 376.22 K, and 4-glazing decreases slightly to 375.87 K. This behaviour can be attributed to two opposing influences. First, each additional

glazing and air gap raises the resistance, decreasing U_t while increasing T_p. Second, under the assumption of refractive index of 1.5 for glazing, each new glazing traps more of the plate's long-wave infrared radiation and re-radiates it back, boosting the effective incident heat flux and tending to increase T_p.

For the 2-glazing layer configuration, these effects balanced out so that the trapping of long-wave radiation just outweighs the added insulation, driving T_p to its highest value. A third layer of glazing provides additional insulation as shown by the value of U_t and significantly improves the trapping of long-wave infrared radiation, but it also resulted in lower energy reached to absorber plate due to optical losses, resulting in a slight reduction in T_p. Adding a fourth glazing tilts the balance toward optical losses, as the drop in T_p is observed, thus overtakes the incremental re-radiation.

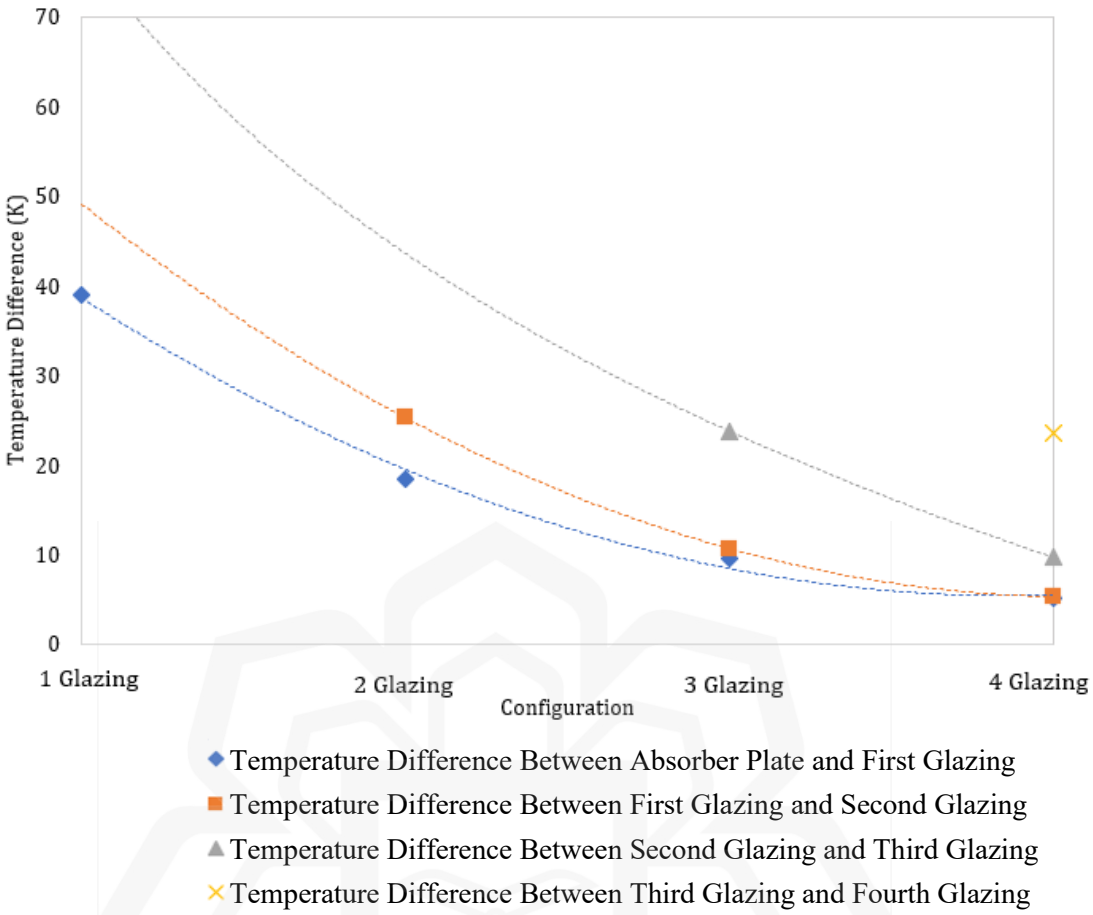

Figure 4.3 The trend of the temperature difference between the absorber plate and each successive glazing layers.

Figure 4.3 shows that as the number of glazing layers increases, the temperature difference (ΔT) between all successive layers decreases consistently. This confirms that each additional glazing layer enhances insulation and diminishes heat loss. The temperature difference from the absorber plate to the first glazing layer decreases sharply as more glass layers are added. For the 1-glazing configuration, the temperature drops approximately 39.00 K, indicating significant heat transfer from the plate to the glazing. When two glazing layers are installed, the drop of the temperature between absorber plate and first glazing is cut approximately by half, to 18.45 K. Adding a third layer of glass reduces the drop to only 9.46 K, and with four glazing layers in place, the temperature change is very small, at only 5.12 K, indicating that glazing most

effectively blocks heat from the plate at starting at 2- and 3-glazing layers configurations, but the effect diminishes for 4-glazing.

Optically, each glazing plays the roles of transmitting the incoming short wave solar radiation while reflecting or absorbing the long-wave radiation from the warmer surfaces below. As glazing layer accumulate and the absorber plate and inner glazing have higher temperatures as shown in Fig. 4.3, internal reflections and trapping of long-wave radiation intensify, further reducing net ΔT. Hence, the temperature drops are gradually distributed across the inner layers. For example, in the 4-glazing setup, the temperature drop across the first, second, and third air gap is around 5.12 K, 5.29 K, and 9.64 K, respectively, while the fourth gap increases significantly, about 23.53 K.

The steepest temperature difference therefore shifts toward the outermost gap, highlighting that the final barrier to convective and radiative losses lies at the glass-air interface. Since the greatest thermal drop remains at the outermost layer, enhancement such as low emissivity coatings or inert gas fills in that gap can further reduce the total heat loss more effectively than simply adding more glass. While each additional glazing layer increases insulation, diminishing returns set in by the third or fourth layer. Therefore, balancing optical and thermal considerations with cost and performance suggests that a 2-glazing configuration is the most cost-effective method for minimizing total top surface heat loss.

Table 4-4 and Figure 4.4 show that the surface incident radiation on the absorber plate peaks at 2-glazing configuration and start to decline gradually with the addition of glazing layers. As mentioned in Section 3.5, the value surface incident radiation, in W was obtained using the surface integral report function of area-weighted average in ANSYS Fluent. When a second glazing layer is introduced, the absorber plate is observed at its highest net incident radiation because each glazing not only transmits the incoming short-wave solar beam but also traps a portion of the absorber's long-wave radiation due to the greenhouse effect. However, adding a third and fourth pane yields only marginal benefit, as it slightly reduces the absorber's net incident radiation, because each extra glazing also cause optical loss despite the greenhouse effect is slightly more significant. Thus, 2-glazing yields the best balance between enhanced long-wave re-radiation and minimized short-wave radiation losses.

Table 4-4 The distribution of surface incident radiation of FPSC for number of glazing layer configurations.

Surface Incident Radiation (W)	**Absorber Plate**	**First Glazing**	**Second Glazing**	**Third Glazing**	**Fourth Glazing**
Configuration:					
1-glazing	169.18	410.15	-	-	-
2-glazing	170.83	395.45	416.93	-	-
3-glazing	170.47	388.28	397.05	417.61	-
4-glazing	169.73	384.28	388.39	397.03	417.61

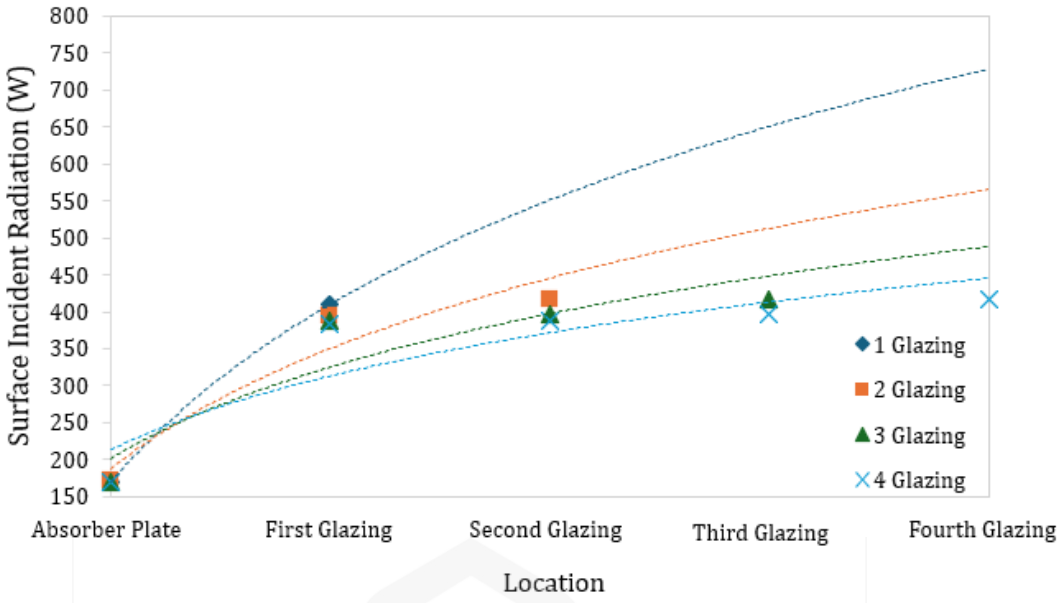

Figure 4.4 The surface incident radiation of absorber plate and each glazing layers, obtained from Anys Fluent.

The distribution of incident radiation through the glazing is also influenced by the number of glazing layers. Each glass layer transmits solar irradiance to the surfaces below with the assumption of an ideal refractive index of 1.5 for glazing. Adding more layers lengthens the radiative path and increases internal reflections within the glazing system, which can affect the amount of incident radiation reaching the interior surfaces.

Across all of the configurations, the outermost glazing have the highest incident radiation across all configurations while each successive layer closer to the absorber shows a gradual decrease. Every glazing surface both reflect the incoming beam and exchanges radiation with its neighbors. Some of the radiation reflected back down from the hotter lower surfaces will be intercepted by the glazing above, increasing their net incident beyond just the direct sunlight.

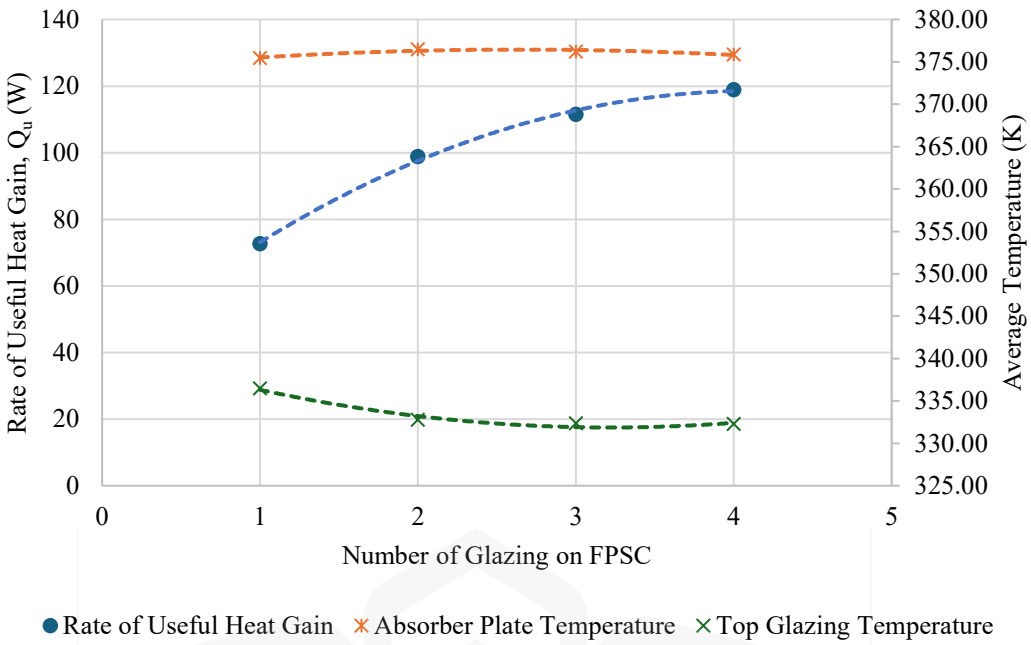

Figure 4.5 The obtained rate of useful heat gain, Q_u of each glazing layer configuration.

Table 4-5 The percentage rate of change of Q_u for each configuration.

Configurations	Percentage rate of change of Q_u (%)
1 Glazing to 2 Glazing	35.87
2 Glazing to 3 Glazing	12.88
3 Glazing to 4 Glazing	6.63

Based on the Table 4-5 and Figure 4.5, the rate of useful heat gain, Q_u, for each glazing configuration, obtained using Equation (30), shows that the largest increase occurs between the 1- and 2-glazing layer configurations, from 72.67 W to 98.77 W, resulting in 35.87% of increase. Meanwhile, the rate of increase becomes smaller starting from 2-glazing to 3-glazing (12.88%) and 3-glazing to 4-glazing (6.63%). Although adding more glazing layers results in higher Q_u values, the diminishing rate of increase indicates that 2 glazing layer configuration provides the most significant improvement in useful heat gain among the tested configurations of the number of glazing thicknesses. Even as the value of U_t decrease and Q_u is increasing as more

glazing layers is added, the value of T_p also start to diminish after the peak value of T_p of 2-glazing layer configurations.

Although each additional glazing lowers U_t by improving insulation and increases the share of radiation trapped among the glazing themselves due to greenhouse effect, it also introduce more optical losses. From a performance and cost-benefit standpoint, two layers appear to strike the best balance between minimizing top heat losses and maximizing radiative input to the absorber as discussed. When glazing is added to FPSC, the greenhouse effect occurs, where the absorber plate emits long-wave radiation, but the glazing traps and re-emits some of that energy back to the plate. As more glazing layers are used, this mechanism becomes stronger, altering the amount of radiation that actually reaches both the absorber and the glazing.

In summary, the balance between of U_t and surface incident radiation explains why 2-glazing yields the highest absorber temperature. It achieves an optimal greenhouse effect by trapping long wave radiation, while still maintaining relatively low optical losses as well as enhanced thermal insulation from lower U_t. By contrast, 3- and 4-glazing shift the balance further toward greenhouse effect enhancement, but it also yields increasing optical losses The single glazing setup, with the highest U_t and lowest incident radiation, clearly underperforms, resulting in the lowest absorber temperature and highest top heat loss coefficient.

In practice, the 2-glazing configuration offers the most feasible balance between efficiency and cost in design. It enhances the FPSC performance without considerably increasing the fabrication cost, system weight or optical losses, making it suitable for both domestic and small-scale industrial solar thermal applications. Therefore, the 2-glazing configuration not only achieves the best thermal performance but also

represents the most technically and economically viable option among the studied setups.

4.2 GLAZING THICKNESS

For the study of glazing thickness, the 2-glazing layer configuration is selected based on the justification of the parameters earlier. Table 4-6 and Figure 4.6 show the obtained top heat loss coefficient, U_t for the study of glazing thickness on FPSC. The thickness of glazing can affect the transmittance of the irradiance and the insulation effect, based on the top heat loss coefficient, U_t. The top heat loss coefficient, U_t is expected to decrease with increasing glazing thickness, as thickness directly influences its calculation, as shown in equations (11), (12), (27), and (28). Consequently, a higher absorber plate temperature is expected. The second glazing layer is referred to as the top glazing.

Table 4-6 The top heat loss coefficient, U_t for each glazing thickness configuration.

Configurations	**Top Heat Loss Coefficients, U_t ($W\ m^{-2}\ K^{-1}$)**
2-mm	4.43
3-mm	4.38
4-mm	4.33
5-mm	4.28

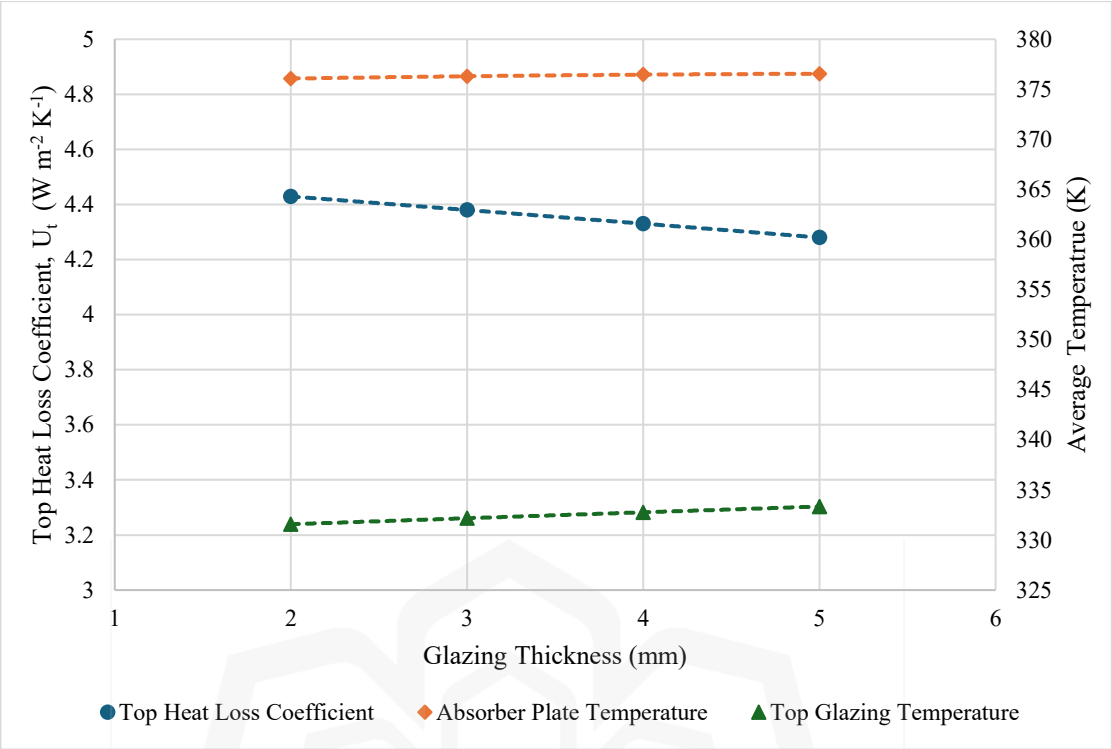

Figure 4.6 The trend of top heat loss coefficient and the trend of the temperature of absorber plate, first glazing and second glazing layer.

Table 4-7 The average temperature of absorber and glazing layers for each glazing thickness configurations.

Configurations	**Average Absorber Plate Temp, T_p (K)**	**Average First Glazing Temp, T_{g1} (K)**	**Average Second Glazing Temp, T_{g2} (K)**
2 mm Glazing	376.08	356.75	331.57
3 mm Glazing	376.29	357.51	332.18
4 mm Glazing	376.48	358.03	332.77
5 mm Glazing	376.55	358.52	333.34

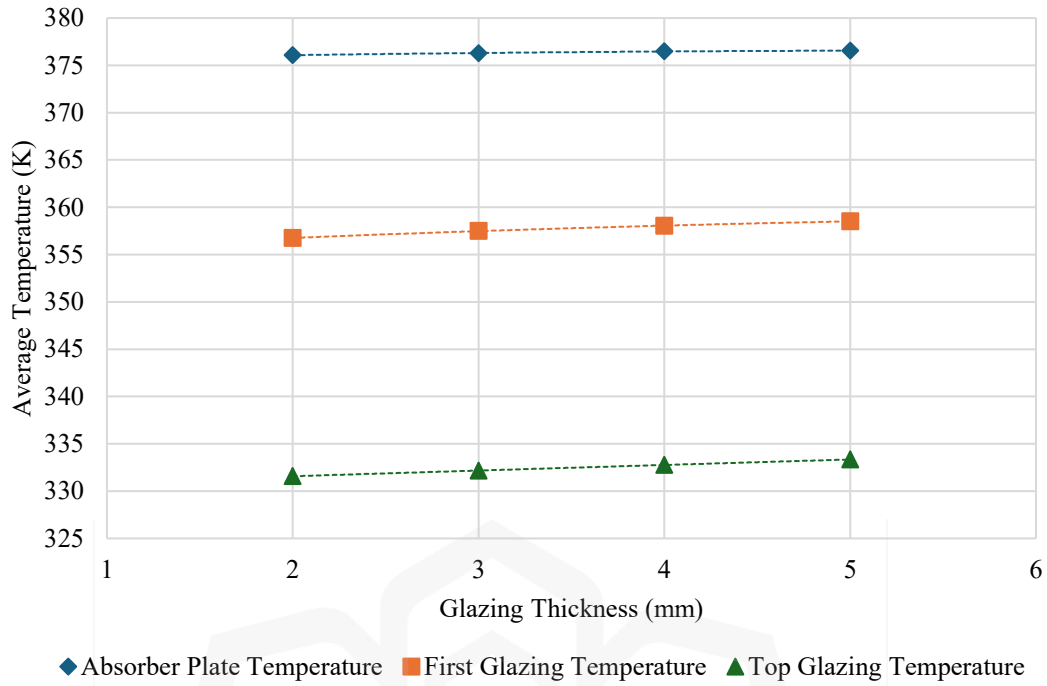

Figure 4.7 The average temperature of absorber and glazing layers for glazing layers configurations.

Table 4-6 and Figure 4.6 show the obtained U_t for each glazing thickness for 2-glazing layer FPSC. It can be observed that the U_t decreases as the thickness of glazing increases. This trend can be attributed by the higher temperature of absorber plate and the glazing layers, as this can influence the convective and radiative heat transfer coefficient based on the equations (11), (12), (27) and (28). As the temperatures of both the absorber and the glazing increase, the value of h_c and h_r increase based on the equations (13) to (26). This increase the total thermal resistance, and since U_t is the inverse of that resistance, U_t therefore decreases.

Additionally, Table 4-7 and Figure 4.7 show the average temperatures of the absorber plate and two glazing layers for different glazing thicknesses in a solar collector system. As glazing thickness increases, the average absorber plate temperature also increases, starting from 376.08 K for 2-mm thickness and peaking at 376.55 K for

5-mm. This trend suggests that moderate increases in glazing thickness enhance thermal insulation, reducing heat loss from the absorber and allowing it to retain more heat.

Table 4-8 The rate of change of U_t for each glazing thickness configuration

Configurations	**Rate of change of U_t (%)**
2 mm glazing to 3-mm glazing	1.11
3-mm glazing to 4-mm glazing	1.14
4-mm glazing to 5-mm glazing	1.16

It is observed that the rate of change for glazing thickness configuration, as shown in Table 4-8, is more gradual compared to the rate of change of U_t for number of glazing layer configurations from Table 4-3. For number of glazing layer configuration, a huge rate of change was observed (ranging from 6.63 % to 35.87 %) meanwhile the thickness of glazing configurations only account for small changing rate, (ranging from 1.11 % to 1.16 %). This means that the thickness of the glazing layer has a very small impact on the top heat loss compared to the number of glazing layer configurations, even though both configurations reduce the value of U_t, however, as both the thickness and the number of glazing layers increase, the reduction in top heat loss occurs at different rates, indicating that the number of layers plays a more significant role in minimizing heat loss.

The rate of change of U_t with respect to glazing thickness is important because it helps identify the point at which increasing thickness no longer provides significant improvement. Understanding this relationship enables designers to select a glazing thickness that enhances thermal insulation without unnecessary material use or added optical losses. This consideration ensures a more cost-effective and efficient FPSC design by balancing performance gains with practical manufacturing and economic constraints.

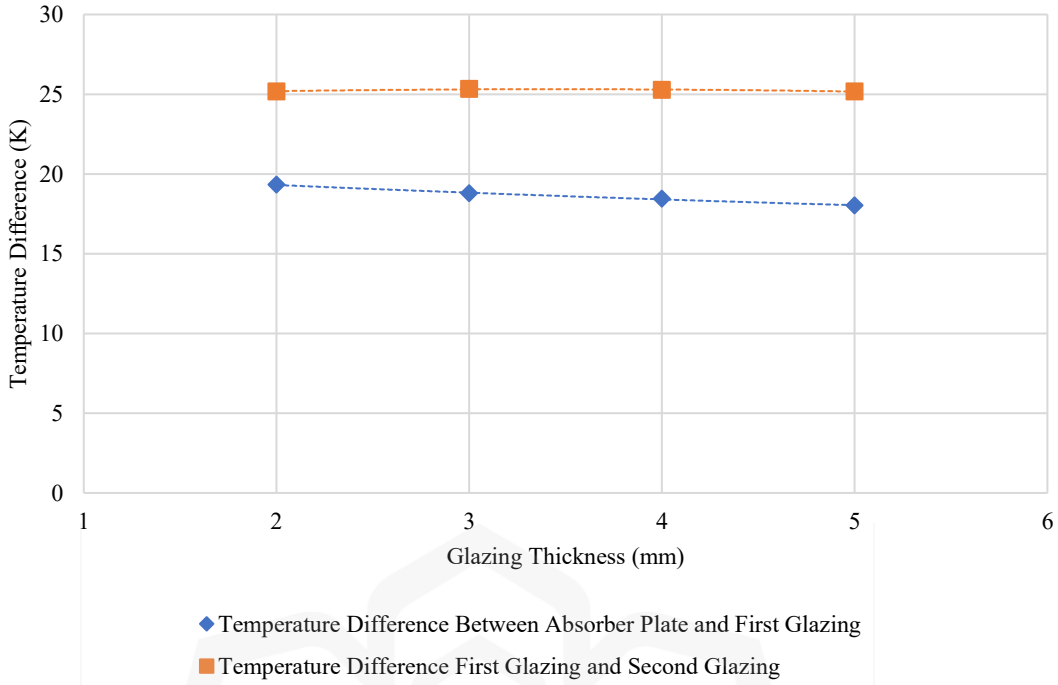

Figure 4.8 The temperature difference between the absorber plate and each glazing layers of FPSC.

As shown in Figure 4.8, the temperature difference (ΔT) between the absorber plate and the first glazing layer decreases slightly with increased glazing thickness, from 19.33 K to 18.03 K. This gradual reduction in ΔT suggests improved thermal insulation, as thicker glazing contributes to greater thermal resistance within the system. The glazing thickness, L_g, appears in the equations for the top heat loss coefficient, U_t. As L_g increases, additional thermal resistances are introduced in series, thereby increasing the total resistance. Since U_t is the inverse of the total resistance, a higher resistance leads to a lower U_t, which indicates improved effectiveness in reducing heat transfer through the top of the collector.

As glazing thickness increases, the slight reduction in ΔT between the absorber plate and the first glazing layer may also be influenced by the optical behavior of the glazing. The glazing has a refractive index of 1.5, which causes some portion of

incoming short-wave solar radiation to reflect at each interface. More interfaces due to thicker glazing lead to slightly more cumulative reflection and reduce solar transmittance reaching the absorber plate. However, thicker glazing also contributes to the better greenhouse effect by trapping more long-wave radiation from the absorber plate, as well as increasing overall thermal resistance, thus lowering U_t. In this scenario, the enhanced greenhouse trapping and increased thermal resistance outweigh the modest optical losses, resulting in a lower ΔT between the absorber and the first glazing layer. Essentially, with thicker glazing, less solar energy escapes outward and more is retained internally, leading to reduced ΔT and improved system insulation.

By contrast, the temperature difference between the first and second glazing layers remains nearly constant, at 25.18 K, 25.33 K, 25.27 K, and 25.18 K for glazing thicknesses of 2-mm, 3-mm, 4-mm, and 5-mm, respectively. This minimal fluctuation indicates that, beyond the first glazing layer, increasing glazing thickness has a negligible effect on inter-layer ΔT.

Table 4-9 The distribution of surface incident radiation of FPSC for glazing thickness configurations.

Configurations	**Absorber Plate (W)**	**First Glazing (W)**	**Second Glazing (W)**
2-mm Glazing	170.03	395.15	418.68
3-mm Glazing	170.68	395.72	418.04
4-mm Glazing	170.83	395.45	416.93
5-mm Glazing	170.95	395.16	415.86

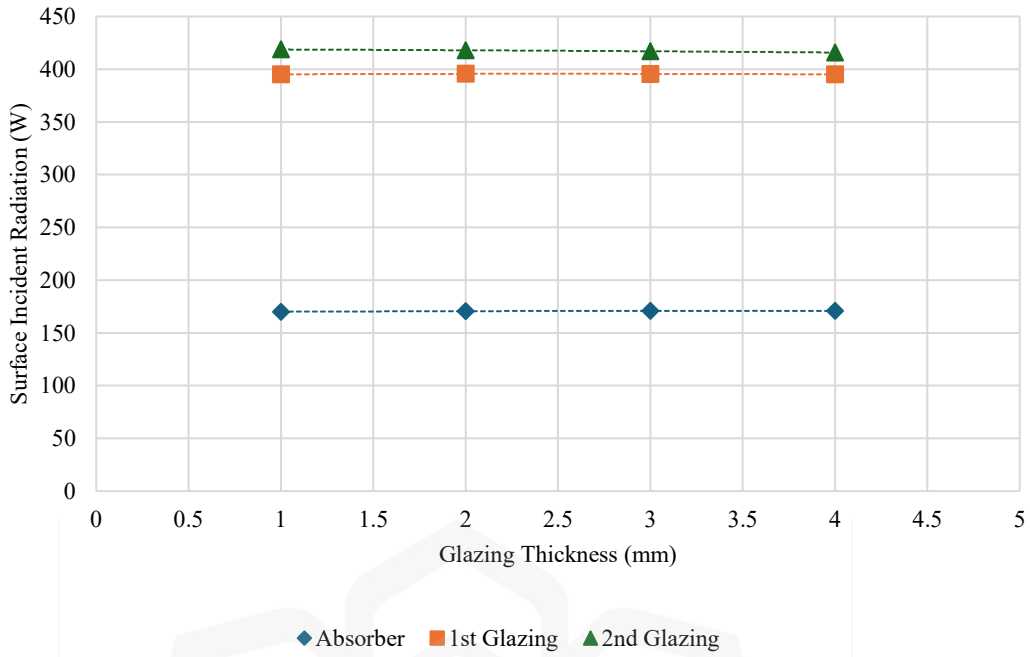

Figure 4.9 The surface incident radiation of absorber plate and each glazing layers, obtained from Anys Fluent.

Table 4-9 and Figure 4.9 show a minimal change in incident radiation on the absorber plate as the glazing thickness increases ranging from 170.03 W at 2-mm to 170.95 W at 5-mm. This trend supports the discussion of enhanced greenhouse effect of heat trapping: thicker glazing absorbs and re-emits more long-wave heat back into the collector, thus trapping the heat and reducing thermal losses. As a result, slightly more energy is retained by the absorber despite a minor reduction in direct solar transmission through the glass. However, the net gain is minimal (less than 1 W), indicating that glazing thickness in this range does not significantly affect the total radiation absorbed by the plate.

The surface incident radiation on the first and second glazing layer also yield minimal fluctuations and decreases, respectively. The small changes in glazing thickness (from 2-mm to 5-mm) yield only marginal decreases in incident radiation on both glazing layers. However, the enhanced internal heat retention, due to greenhouse

effect and convective loss, provides a slight benefit to absorber performance, illustrating how glazing thickness mediates a balance between optical attenuation and thermal insulation.

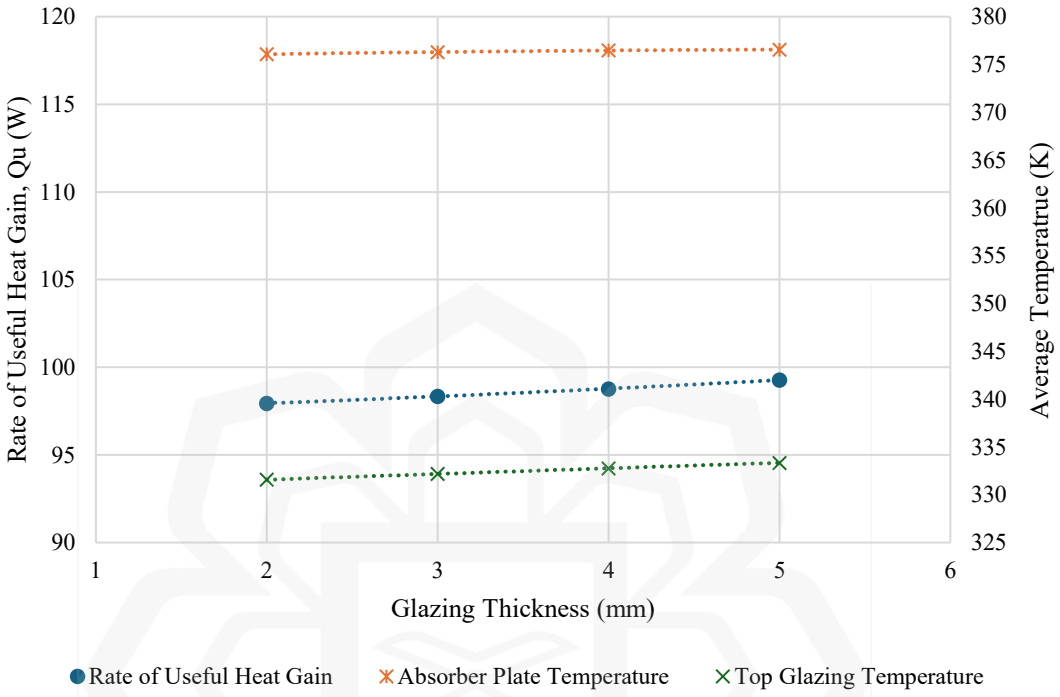

Figure 4.10 The obtained rate of useful heat gain, Q_u of each glazing thickness configuration.

Table 4-10 The percentage rate of change of Q_u for each glazing thickness configuration.

Configurations	Percentage rate of change of Q_u (%)
2-mm to 3-mm	0.41
3-mm to 4-mm	0.43
4-mm to 5-mm	0.51

It is observed that the Q_u increase gradually as the glazing is thicker, starting from 97.95 W for 2-mm to 98.35 W for 3-mm, resulting in 0.41 % of increase. The increase continue with 98.77 W for 4-mm (0.43 % increase) and lastly 99.28 W for 5-mm, resulting in the largest increase rate, at 0.51 %. The rate of change is small, but has

gradual increase starting, indicating that the Q_u is not significantly affected by the increasing glazing thickness.

Up to 5-mm glazing thickness, the results observed to suggest that the performance of FPSC is improved with the increasing value of T_p, U_t and Q_u, as well as surface incident radiation. However, the trend of the increase is shown to be minimal, suggesting that increasing the thickness provide less significant improvements to the performance of FPSC, compared to the number of glazing layers.

In summary, considering both performance and economic feasibility, the configuration with 2-glazing layers demonstrates the most effective improvement among all configurations. It provides the optimal balance between the T_p, U_t, ΔT, distribution of surface incident radiation and Q_u as discussed in this chapter. Beyond this, further addition of glazing layers yields diminishing returns, as the optical losses begin to offset the thermal insulation benefits Similarly, the analysis on glazing thickness shown that the 5-mm glazing offers a practical balance in maintaining sufficient transmittance while also enhancing insulation, making it an efficient and cost-effective choice for FPSC design. Overall, the findings from this chapter establish that both the 2-glazing configuration and the 5-mm thickness provide the best overall balance between performance efficiency and economic practicality.

CHAPTER FIVE

CONCLUSION

In this study, the interaction between the number of glazing layer and glazing thickness configuration, top heat loss, absorber temperature, and internal radiation was systematically examined under ideal optical conditions. As glazing layers and glazing thickness increase, the overall top heat loss coefficient, U_t decrease considerably for glazing number and less so for glazing thickness. For glazing number configuration, each additional air gap and glazing adds significant thermal resistance via convection and radiation insulation. Additionally, adding more glazing and increasing its thickness enhance the greenhouse effect by trapping long-wave thermal radiation, but also introduces additional optical losses due to increased internal reflections at each glazing layers.

From the result and discussion, the 2-glazing layer configuration resulted in the balanced of high absorber temperature and reduced heat loss, outperforming 1-, 3-, and 4-glazing layer configurations. Although its U_t is higher than the 3- and 4-glazing model's, the 2-glazing design achieves the highest absorber temperature 376.48 K (103.33 °C) . In the 2-glazing study, 5-mm glazing yields the peak absorber temperature at 376.55 K (103.40 °C), follow closely by 4-mm glazing, which is used in the number of glazing layer's study. The impact of glazing number and thickness can be attributed to the top heat loss coefficient, U_t which is the combination of convective, radiative and conductive heat transfer within the FPSC, optical loss through transmission and reflection of short-wave radiation, and the greenhouse effect, where long-wave radiation from the absorber plate is retained. The configuration of 2-glazing number

with 5-mm glazing thickness is demonstrated to provide a balanced approach regarding the mentioned attributes.

Thicker glazing correlates with slightly improved heat retention, with a notable increase beyond 4-mm. While the gains are small, they could be significant for precision thermal systems. To optimize design and cost, further investigation into thicknesses above 5-mm and comprehensive error analysis is recommended.

To enhance the thermal performance of FPSC, future designs should incorporate high-performance materials beyond those used in this simulation, which are based on commercially available components sourced from existing catalogues and previous studies. While these materials provide a realistic baseline, more advanced options could yield better insulation and energy efficiency. It is also important to note that the findings of this study are specific to Malaysia's hot climate, which have high ambient temperatures and solar intensity influence performance. Therefore, boundary conditions in simulations must be adapted to suit the environmental characteristics of different regions. Additionally, this study assumes air as the medium between glazing layers; however, using alternative gases with lower thermal conductivity or implementing vacuum conditions may further reduce heat losses.

An optimal FPSC design requires a careful balance between the number of glazing layers to reduce the U_t, while leveraging the greenhouse effect and minimizing short-wave optical losses. This balance is particularly important in hot climates like Malaysia's, where thermal and optical management must be optimized concurrently. By integrating advanced materials and tailoring the number of glazing layers to the climate and design goals, future solar collectors can significantly improve their efficiency by minimizing thermal losses while maximizing solar energy capture.

Future study could focus on extending the present study by incorporating experimental validation of the simulated results to verify the predicted absorber temperature and U_t under real outdoor conditions. Further analysis could also explore the combined effects of glazing material properties, such as solar transmittance and emissivity, to optimize both optical and thermal performance. Additionally, investigating dynamic environmental factors such as varying solar irradiance, wind velocity, and angle of incidence throughout the day could provide a more comprehensive understanding of collector performance under realistic operating conditions. Finally, future studies can enhance the present CFD model by applying advanced radiation models, such as Monte Carlo, to capture complex radiative interactions within multilayer glazing systems or using larger number of elements of mesh. The influence of wavelength-dependent solar properties and spectral transmissivity can also be incorporated for greater accuracy for real life setting. Moreover, using transient simulation instead of steady-state analysis would allow investigation of the collector's performance throughout different times of day.

REFERENCES

Abidemi Obatoyinbo Ajayi, Chijioke Paul Agupugo, Chinonso Nwanevu, & Chuku Chimziebere Patience. (2024). Review of penetration and impact of utility solar installation in developing countries: policy and challenges. International Journal of Frontiers in Engineering and Technology Research, 7(2), 011–024.

Akhtar, N., & Mullick, S. C. (1999). Approximate method for computation of glass cover temperature and top heat-loss coefficient of solar collectors with single glazing. Solar Energy, 66(5), 349–354.

Akhtar, N., & Mullick, S. C. (2012). Effect of absorption of solar radiation in glass-cover(s) on heat transfer coefficients in upward heat flow in single and double glazed flat-plate collectors. International Journal of Heat and Mass Transfer, 55(1–3), 125–132.

Al-Ajlan, S. A., Al Faris, H., & Khonkar, H. (2003). A simulation modeling for optimization of flat plate collector design in Riyadh, Saudi Arabia. Renewable Energy, 28(9), 1325–1339.

Alternative Energy Tutorials. (n.d.). Flat Plate Collector.

Bakari, R., Minja, R. J. A., & Njau, K. N. (2014). Effect of Glass Thickness on Performance of Flat Plate Solar Collectors for Fruits Drying. Journal of Energy, 2014, 1–8.

Barbier, E. (2002). Geothermal energy technology and current status: an overview. Renewable and Sustainable Energy Reviews, 6(1–2), 3–65.

Barone, G., Buonomano, A., Forzano, C., & Palombo, A. (2019). Solar thermal collectors. Solar Hydrogen Production: Processes, Systems and Technologies, 151–178.

Bayod-Rújula, A. A. (2019). Solar photovoltaics (PV). Solar Hydrogen Production: Processes, Systems and Technologies, 237–295.

Bisen, A., Dass, P. P., & Jain, R. (2011). Parametric studies of top heat loss coefficient of double glazed flat plate solar collectors. MIT Int J Mech Eng, 1(2), 71–78.

Buchberg, H., Cation, I., & Edwards, D. K. (1976). Natural Confection in Enclosed Spaces-A Review of Application to Solar Energy Collection. http://heattransfer.asmedigitalcollection.asme.org/

Carlsson, J., Taylor, N., Georgakaki, A., Letout, S., Mountraki, A., Ince, E., Schmitz A., & Gea Bermudez, J. (2024). Clean Energy Technology Observatory: Solar Thermal Energy in the European Union – 2024 Status Report on Technology Development, Trends, Value Chains and Markets. Clean Energy Technology Observatory, JRC139446(EUR 40064).

Cengel, Y. A., & Ghajar, A. J. (2014). Heat and Mass Transfer Fundamentals and Applications 5th Edition: Vol. Fifth Edition.

Chen, C. Q., Diao, Y. H., Zhao, Y. H., Wang, Z. Y., Zhu, T. T., Wang, T. Y., & Liang, L. (2021). Numerical evaluation of the thermal performance of different types of double glazing flat-plate solar air collectors. Energy, 233, 121087.

Chopra, K., Pathak, P. K., Samykano, M., Tyagi, V. V, & Pandey, A. K. (2021). Recent Advancements in Design of Flat Plate Solar Collectors. IOP Conference Series: Materials Science and Engineering, 1127(1), 012007.

Duffie, J. A. ., & Beckman, W. A. . (2013). Solar engineering of thermal processes. Wiley.

Echarri-Iribarren, V., Rizo-Maestre, C., & Sanjuan-Palermo, J. L. (2019). Underfloor heating using ceramic thermal panels and solar thermal panels in public buildings in the Mediterranean: Energy savings and healthy indoor environment. Applied Sciences (Switzerland), 9(10).

Ehrmann, N., & Reineke-Koch, R. (2012). Selectively coated high efficiency glazing for solar-thermal flat-plate collectors. Thin Solid Films, 520(12), 4214–4218.

El Alami, Y., Zohal, B., Nasrin, R., Benhmida, M., Faize, A., & Baghaz, E. (2024). Solar thermal, photovoltaic, photovoltaic thermal, and photovoltaic thermal phase change material systems: A comprehensive reference guide. International Communications in Heat and Mass Transfer, 159, 108135.

Elcioglu, E. B., Genc, A. M., Karadeniz, Z. H., Ezan, M. A., & Turgut, A. (2020). Nanofluid figure-of-merits to assess thermal efficiency of a flat plate solar collector. Energy Conversion and Management, 204, 112292.

Faddouli, A., Hajji, M., Fadili, S., Hartiti, B., Labrim, H., & Habchi, A. (2024). A comprehensive review of solar, thermal, photovoltaic, and thermoelectric hybrid systems for heating and power generation. International Journal of Green Energy, 21(2), 413–447.

Fan, J. C. C., & Bachner, F. J. (1976). Transparent heat mirrors for solar-energy applications.

Fusegi, T., Hyun, J. M., Kuwahara, K., & Farouk, B. (1991). A numerical study of three-dimensional natural convection in a differentially heated cubical enclosure. International Journal of Heat and Mass Transfer, 34(6), 1543–1557.

Genc, A. M., Ezan, M. A., & Turgut, A. (2018). Thermal performance of a nanofluid-based flat plate solar collector: A transient numerical study. Applied Thermal Engineering, 130, 395–407.

Giovannetti, F., Föste, S., Ehrmann, N., & Rockendorf, G. (2014). High transmittance, low emissivity glass covers for flat plate collectors: Applications and performance. Solar Energy, 104, 52–59.

Goodman, R. D., & Menke, A. G. (1975). Effect of cover plate treatment on efficiency of solar collectors. Solar Energy, 17(4), 207–211

Gupta, H. K., Agrawal, G. Das, & Mathur, J. (2015). Investigations for effect of Al2O3–H2O nanofluid flow rate on the efficiency of direct absorption solar collector. Case Studies in Thermal Engineering, 5, 70–78.

Hammarberg, E., & Roos, A. (2003). Antireflection treatment of low-emitting glazings for energy efficient windows with high visible transmittance. Thin Solid Films, 442(1–2), 222–226.

Herrando, M., Wang, K., Huang, G., Otanicar, T., Mousa, O. B., Agathokleous, R. A., Ding, Y., Kalogirou, S., Ekins-Daukes, N., Taylor, R. A., & Markides, C. N. (2023). A review of solar hybrid photovoltaic-thermal (PV-T) collectors and systems. Progress in Energy and Combustion Science, 97, 101072.

Hoel, M., & Kverndokk, S. (1996). Depletion of fossil fuels and the impacts of global warming. Resource and Energy Economics, 18(2), 115–136.

Hsieh, C. K., & Coldewey, R. W. (1974). Study of thermal radiative properties of antireflection glass for flat-plate solar collector covers. Solar Energy, 16(2), 63–72.

Huttrer, G. W. (2021). Geothermal Power Generation in the World 2015-2020 Update Report.

Ihaddadene, N., Ihaddadene, R., & Mahdi, A. (2014). Effect of Glazing Number on the Performance of a Solar Thermal Collector. In International Journal of Science and Research. www.ijsr.net

Ismoilov, M., Xatamova, Z., Rustamov, I., Xolmatov, S., Arabboyev, X., & Ibragimov, N. (2024). Increasing the efficiency of solar water heating installations with flat-flat collectors: optimization of circuit solutions and mode parameters. E3S Web of Conferences, 592.

Jannot, Y., & Coulibaly, Y. (1997). Radiative heat transfer in a solar air heater covered with a plastic film. Solar Energy, 60(1), 35–40.

Jiang, C., Yu, L., Yang, S., Li, K., Wang, J., Lund, P. D., & Zhang, Y. (2020). A review of the compound parabolic concentrator (CPC) with a tubular absorber. In Energies (Vol. 13, Issue 3). MDPI AG.

Joselin Herbert, G. M., Iniyan, S., Sreevalsan, E., & Rajapandian, S. (2007). A review of wind energy technologies. Renewable and Sustainable Energy Reviews, 11(6), 1117–1145.

Kalogirou, S. A. (2004). Solar thermal collectors and applications. In Progress in Energy and Combustion Science (Vol. 30, Issue 3, pp. 231–295).

Kalogirou, S. A. (2014). Flat-plate collector construction and system configuration to optimize the thermosiphonic effect. Renewable Energy, 67, 202–206.

Kannan, N., & Vakeesan, D. (2016). Solar energy for future world: - A review. Renewable and Sustainable Energy Reviews, 62, 1092–1105.

Khoukhi, M., Maruyama, S., Komiya, A., & Behnia, M. (2006). Flat-plate solar collector performance with coated and uncoated glass cover. Heat Transfer Engineering, 27(1), 46–53.

Kim, T., Choi, B. Il, Han, Y. S., & Do, K. H. (2018). A comparative investigation of solar-assisted heat pumps with solar thermal collectors for a hot water supply system. Energy Conversion and Management, 172, 472–484.

Klaiß, H., Köhne, R., Nitsch, J., & Sprengel, U. (1995). Solar thermal power plants for solar countries — Technology, economics and market potential. Applied Energy, 52(2–3), 165–183.

Kocer, A., Yaka, I., Sardogan, G., & Gungor, A. (2015). Effects of Tilt Angle on Flat-Plate Solar Thermal Collector Systems. British Journal of Applied Science & Technology, 9(1), 77–85.

Krane, R. J., & Jessee, J. (1983). Some Detailed Field Measurements for a Natural Convection Flow in a Vertical Square Enclosure. Proceedings of the First ASME-JSME Thermal Engineering Joint Conference, 1, 323–329.

Kumar, A., Said, Z., & Bellos, E. (2020). An up-to-date review on evacuated tube solar collectors. Journal of Thermal Analysis and Calorimetry, 145.

Kumar, R., & Rosen, M. A. (2011). A critical review of photovoltaic–thermal solar collectors for air heating. Applied Energy, 88(11), 3603–3614.

Li, X., Sun, Y., Liu, X., Ming, Y., & Wu, Y. (2024). Development of a comprehensive method to estimate the optical, thermal and electrical performance of a complex PV window for building integration. Energy, 294, 130251.

Liu, Y., Tan, C., Jin, Y., & Ma, S. (2022). Heat collection performance analysis of corrugated flat plate collector: An experimental study. Renewable Energy, 181, 1–9.

Lv, Y., Si, P., Rong, X., Yan, J., Feng, Y., & Zhu, X. (2018). Determination of optimum tilt angle and orientation for solar collectors based on effective solar heat collection. Applied Energy, 219, 11–19.

Makki, A., Omer, S., & Sabir, H. (2015). Advancements in hybrid photovoltaic systems for enhanced solar cells performance. Renewable and Sustainable Energy Reviews, 41, 658–684

Masum, M., & Ali Akbar, M. (2019). The Pacific Ring of Fire is Working as a Home Country of Geothermal Resources in the World. IOP Conference Series: Earth and Environmental Science, 249(1).

Mesa F. (2006). Colector Solar de Placa Plana. Energia Solar.

Moncada, M. L. T., Muñoz, B. C., Yoshida, M. M., & Rodríguez, R. D. (2014). Comparative Experimental Study of New Absorbent Surface Coatings for Flat Plate Solar Collectors. Energy Procedia, 57, 2131–2138.

Morcos, V. H. (1994). Optimum tilt angle and orientation for solar collectors in Assiut, Egypt. Renewable Energy, 4(3), 291–298.

Mullick, S. C., & Samdarshi S K. (1991). S. K. Samdarshi Analytical Equation for the Top Heat Loss Factor of a Flat-Plate Collector With Double Glazing. http://solarenergyengineering.asmedigitalcollection.asme.org/

Mutonga, M. W., & Fujimitsu, Y. (2024). Identification of natural subsurface structures using borehole images, temperature logs and pertinent data: A case study of the Menengai geothermal field, Kenya. Geoenergy Science and Engineering, 237, 212797.

Nahar, N. M., & Garg, H. P. (1980). Free convection and shading due to gap spacing between an absorber plate and the cover glazing in solar energy flat-plate collectors. Applied Energy, 7(1–3), 129–145.

Nahar, N. M., & Guf'ta, J. P. (1989). Studies On Gap Spacing Between Absorber And Cover Glazing In Flat Plate Solar Collectors Free convection Shading Air gap Flat-plate collector Solar energy. In International Journal Of Energy Research (Vol. 13).

National Standards Authority of Ireland (NSAI). (2011). Certificate No. 11/0361 / Grant Sahara Solar Thermal Heating Systems.

Njiri, J. G., & Söffker, D. (2016). State-of-the-art in wind turbine control: Trends and challenges. Renewable and Sustainable Energy Reviews, 60, 377–393.

N'Tsoukpoe, K. E. (2022). Effect of orientation and tilt angles of solar collectors on their performance: Analysis of the relevance of general recommendations in the West and Central African context. Scientific African, 15.

O'Hegarty, R., Kinnane, O., & McCormack, S. J. (2016). Review and analysis of solar thermal facades. Solar Energy, 135, 408–422.

Parida, B., Iniyan, S., & Goic, R. (2011). A review of solar photovoltaic technologies. Renewable and Sustainable Energy Reviews, 15(3), 1625–1636.

Patrick, T. H., Abraham, T. F., Marcel, E., & Alexis, K. (2019). Numerical study of the greenhouse effect in a flat-plate double glazing solar heat collector. Indian Journal of Science and Technology, 12(38), 1–9.

S. O. Amiebenomo, I. I. Omorodion, & J.O. Igbinoba. (2013). View of Prototype Design and Performance Analysis of Solar Clothes Dryer. Asian Review of Mechanical Engineering, 2(1), 35–43.

Sakhaei, S. A., & Valipour, M. S. (2020). Investigation on the effect of different coated absorber plates on the thermal efficiency of the flat-plate solar collector. Journal of Thermal Analysis and Calorimetry, 140(3), 1597–1610.

Samdarshi, S. K., & Mullick, S. C. (1988). An Improved Technique for Computing the Top Heat Loss Factor of a Flat-Plate Collector With a Single Glazing. http://solarenergyengineering.asmedigitalcollection.asme.org/

Senthil, R., Kishore Kumar, K., Rohan Rajendra, K., & Juneja, A. (2021). Enhancement of absorptance of absorber surfaces of a flat plate solar collector using black coating with graphene. Energy Sources, Part A: Recovery, Utilization and Environmental Effects, 43(20), 2595–2608.

Shariah, A. M., Rousan, A., Rousan, K. K., & Ahmad, A. A. (1999). Effect of thermal conductivity of absorber plate on the performance of a solar water heater. Applied Thermal Engineering, 19(7), 733–741.

Solar Photovoltaic Technology Basics | Department of Energy. (n.d.). Retrieved April 29, 2024, from https://www.energy.gov/eere/solar/solar-photovoltaic-technology-basics

Struckmann, F. (2008). Analysis of a Flat-plate Solar Collector.

Subiantoro, A., & Ooi, K. T. (2013). Analytical models for the computation and optimization of single and double glazing flat plate solar collectors with normal and small air gap spacing. Applied Energy, 104, 392–399.

Sukhatme, S. (2009). Solar Energy: Principles of Thermal Collection and Storage.

Sup, B. A., Ali, T. Z. S., Zainudin, M. F., & Bakar, R. A. (2014). Experimental study of water heating efficiency between aluminium and copper absorber plate in solar flat plate collector. Applied Mechanics and Materials, 660, 709–713.

Swinbank, W. C. (1963). Long-wave radiation from clear skies.

Tian, M., Su, Y., Zheng, H., Pei, G., Li, G., & Riffat, S. (2018). A review on the recent research progress in the compound parabolic concentrator (CPC) for solar energy applications. Renewable and Sustainable Energy Reviews, 82, 1272–1296.

Tian, Y., & Zhao, C. Y. (2013). A review of solar collectors and thermal energy storage in solar thermal applications. Applied Energy, 104, 538–553.

Tiwari, A. K., Chatterjee, K., Agrawal, S., & Singh, G. K. (2023). A comprehensive review of photovoltaic-thermal (PVT) technology: Performance evaluation and contemporary development. Energy Reports, 10, 2655–2679.

Tsilingiris, P. T. (1999). Heat transfer analysis of low thermal conductivity solar energy absorbers. www.elsevier.com/locate/apthermeng

Tsilingiris, P. T. (2002). Back absorbing parallel plate polymer absorbers in solar collector design. Energy Conversion and Management, 43(1), 135–150.

Tsoutsos, T., Gekas, V., & Marketaki, K. (2003). Technical and economical evaluation of solar thermal power generation. Renewable Energy, 28(6), 873–886.

Ukoba, K., Yoro, K. O., Eterigho-Ikelegbe, O., Ibegbulam, C., & Jen, T. C. (2024). Adaptation of solar energy in the Global South: Prospects, challenges and opportunities. In Heliyon (Vol. 10, Issue 7). Elsevier Ltd.

Vignarooban, K., Xu, X., Arvay, A., Hsu, K., & Kannan, A. M. (2015). Heat transfer fluids for concentrating solar power systems – A review. Applied Energy, 146, 383–396.

Vutukuru, R., Pegallapati, A. S., & Maddali, R. (2019). Suitability of various heat transfer fluids for high temperature solar thermal systems. Applied Thermal Engineering, 159, 113973.

Wang, P., Zhang, Y., & Guo, Z. (2017). Numerical study of three-dimensional natural convection in a cubical cavity at high Rayleigh numbers. International Journal of Heat and Mass Transfer, 113, 217–228.

Witmer, L., & Fedkin, M. (n.d.). 3.1 Overview of Flat Plate Collectors | EME 811: Solar Thermal Energy for Utilities and Industry. Retrieved June 16, 2025, from https://www.e-education.psu.edu/eme811/node/685

Yoo, D. H., Hong, K. S., & Yang, H. S. (2007). Study of thermal conductivity of nanofluids for the application of heat transfer fluids. Thermochimica Acta, 455(1–2), 66–69.

Zeghıb, İ. İ., & Chaker, A. (2015). Modeling and Simulation of a Solar Thermal System for Domestic Space Heating Using Radiators Low Temperature. International Journal Of Renewable Energy Research, 5(1), 266–276. https://dergipark.org.tr/en/pub/ijrer/issue/16072/168011

Zhang, C., Li, N., & An, G. (2024). Review of Concentrated Solar Power Technology Applications in Photocatalytic Water Purification and Energy Conversion: Overview, Challenges and Future Directions. In Energies (Vol. 17, Issue 2). Multidisciplinary Digital Publishing Institute (MDPI).

Zhang, P., Yue, C., Li, Y., Tang, X., Liu, B., Xu, M., Wang, M., & Wang, L. (2024). Revisiting the land use conflicts between forests and solar farms through energy efficiency. Journal of Cleaner Production, 434, 139958.

APPENDIXES

Additional Data Tables

Using the equation (10) to equation (26), the value of T_m, V, P_r, R_a, N_u, heat transfer coefficient of natural convection and radiation, and Q_o for the investigation of number of glazing layers are calculated as shown in the table below. All of the calculations are done in the Microsoft Excel software.

Table 1 The value of arithmetic mean of temperature of each layer.

Configurations	T_{m1} **(K)**	T_{m2} **(K)**	T_{m3} **(K)**	T_{m4} **(K)**
1 Glazing	361.38402	-	-	-
2 Glazing	375.77831	349.90909	-	-
3 Glazing	376.12311	367.49989	348.10122	-
4 Glazing	381.92492	377.16859	367.94744	348.23569

Table 2 The value of K, V, P_r and R_a for the layer between absorber plate and first glazing.

Configurations	K_1	V_1	P_{r1}	R_{a1}
1 Glazing	0.032180	2.2039×10^{-5}	0.903521863	276481.5437
2 Glazing	0.033302	2.357×10^{-5}	0.902504097	118403.973
3 Glazing	0.033328	2.3607×10^{-5}	0.902480199	29663.13287
4 Glazing	0.033776	2.423×10^{-5}	0.902081321	15609.91147

Table 3 The value of N_u, h_{cpg} and h_{rpg} for the layer between absorber plate and first glazing.

Configurations	N_{u1}	h_{cpg1} **(W m^{-2} K^{-1})**	h_{rpg1} **(W m^{-2} K^{-1})**
1 Glazing	1.144107845	0.736358105	10.74349
2 Glazing	0.929766406	0.61925327	12.04543154
3 Glazing	3.067850349	2.044921839	12.06861307
4 Glazing	2.609590683	1.762856391	12.6352691

Table 4 The value of K, V, P_r and R_a for the layer between first glazing and second glazing.

Configurations	K_2	V_2	P_{r2}	R_{a2}
1 Glazing	-	-	-	-
2 Glazing	0.031277818	2.08456×10^{-5}	0.904362686	214068.608
3 Glazing	0.032658304	2.26851×10^{-5}	0.903084567	67985.8434
4 Glazing	0.033409174	2.37198×10^{-5}	0.902407869	33047.7044

Table 5 The value of N_u, h_{cpg} and h_{rpg} for the layer between first glazing and second glazing.

Configurations	N_{u2}	h_{cpg2} (W m^{-2} K^{-1})	h_{rpg2} (W m^{-2} K^{-1})
1 Glazing	-	-	-
2 Glazing	1.033817908	0.64671137	9.733601083
3 Glazing	3.780984889	2.469611064	11.25960777
4 Glazing	3.152528992	2.106467809	12.16971207

Table 6 The value of K, V, P_r and R_a for the layer between second glazing and third glazing.

Configurations	K_3	V_3	P_{r3}	R_{a3}
1 Glazing	-	-	-	-
2 Glazing	-	-	-	-
3 Glazing	0.031134888	2.06598×10^{-5}	0.904497667	202655.6133
4 Glazing	0.032693185	2.27326×10^{-5}	0.903052853	70386.89206

Table 7 The value of N_u, h_{cpg} and h_{rpg} for the layer between second glazing and third glazing.

Configurations	N_{u3}	h_{cpg3} (W m^{-2} K^{-1})	h_{rpg3} (W m^{-2} K^{-1})
1 Glazing	-	-	-
2 Glazing	-	-	-
3 Glazing	1.01314947	0.630885908	9.581221256
4 Glazing	3.814199573	2.493966615	11.30102358

Table 8 The value of K, V, P_r and R_a for the layer between third glazing and fourth glazing.

Configurations	K_4	V_4	P_{r4}	R_{a4}
1 Glazing	-	-	-	-
2 Glazing	-	-	-	-
3 Glazing	-	-	-	-
4 Glazing	0.031145526	2.06736×10^{-5}	0.904487604	203422.0474

Table 9 The value of N_u, h_{cpg} and h_{rpg} for the layer between third glazing and fourth glazing.

Configurations	N_{u4}	h_{cpg4} (W m^{-2} K^{-1})	h_{rpg4} (W m^{-2} K^{-1})
1 Glazing	-	-	-
2 Glazing	-	-	-
3 Glazing	-	-	-
4 Glazing	1.014586557	0.631996637	9.592479148

Table 10 The value of the radiation heat transfer coefficient at the top glazing.

Configurations	**Radiation Heat Transfer Coefficient at The Top Glazing (W m^{-2} K^{-1})**
1 Glazing ($h_{rg1a)}$	7.547091285
2 Glazing ($h_{rg2a)}$	7.393714472
3 Glazing ($h_{rg3a)}$	7.368472764
4 Glazing ($h_{rg4a)}$	7.37059689

Table 11 The value of the rate of heat loss, Q_o for number of glazing layers study.

Configurations	Q_o **(W)**
1 Glazing	69.69338362
2 Glazing	48.03694135
3 Glazing	34.63892368
4 Glazing	30.41254688

For the investigation of glazing thickness of FPSC, the value of T_m, V, P_r, R_a, N_u, heat transfer coefficient of natural convection and radiation, and Q_o for the investigation of number of glazing layers are calculated as shown in the table below.

Table 12 The value of arithmetic mean of temperature of each glazing thickness.

Configurations	T_{m1} **(K)**	T_{m2} **(K)**
2 mm Glazing	365.32727	342.36440
3 mm Glazing	375.54260	349.56908
4 mm Glazing	375.77831	349.90909
5 mm Glazing	365.50415	342.66124

Table 13 The value of K, V, P_r and R_a for the layer between absorber plate and first glazing.

Configurations	K_1	V_1	P_{r1}	R_{a1}
2 mm Glazing	0.032489	2.24549×10^{-5}	0.903239074	121677.4059
3 mm Glazing	0.033283	2.35446×10^{-5}	0.902520448	120036.8471
4 mm Glazing	0.033302	2.357×10^{-5}	0.902504097	118403.997
5 mm Glazing	0.032503	2.24736×10^{-5}	0.903226461	119573.9814

Table 14 The value of N_u, h_{cpg} and h_{rpg} for the layer between absorber plate and first glazing.

Configurations	N_{u1}	h_{cpg1} **(W m^{-2} K^{-1})**	h_{rpg1} **(W m^{-2} K^{-1})**
2 mm Glazing	0.914152385	0.593994407	11.06682465
3 mm Glazing	0.932891071	0.620993728	12.02302632
4 mm Glazing	0.929766456	0.6192533	12.04543135
5 mm Glazing	0.910007108	0.591552247	11.08264297

Table 15 The value of K, V, P_r and R_a for the layer between first glazing and second glazing.

Configurations	K_2	V_2	P_{r2}	R_{a2}
2 mm Glazing	0.030680039	2.09923×10^{-5}	0.904930684	188603.0219
3 mm Glazing	0.031250952	2.18496×10^{-5}	0.904388019	194802.2027
4 mm Glazing	0.031277818	2.18804×10^{-5}	0.904362687	194299.9335
5 mm Glazing	0.030703622	2.10177×10^{-5}	0.904908101	188472.0233

Table 16 The value of N_u, h_{cpg} and h_{rpg} for the layer between first glazing and second glazing.

Configurations	N_{u2}	h_{cpg2} (W m^{-2} K^{-1})	h_{rpg2} (W m^{-2} K^{-1})
2 mm Glazing	0.978109034	0.600168464	9.114204269
3 mm Glazing	1.005535708	0.628478956	9.70524443
4 mm Glazing	1.005659939	0.629096965	9.733600628
5 mm Glazing	0.978667065	0.60097247	9.137975824

Table 17 The value of the radiation heat transfer coefficient at the top glazing.

Configurations	**Radiation Heat Transfer Coefficient at The Top Glazing (W m^{-2} K^{-1})**
2 mm Glazing (h_{rg1a})	7.192166918
3 mm Glazing (h_{rg2a})	7.382184898
4 mm Glazing (h_{rg3a})	7.393714221
5 mm Glazing (h_{rg4a})	7.201388503

Table 18 The value of the rate of heat loss, Q_o for glazing thickness study.

Configurations	Q_o **(W)**
2 mm Glazing	39.23523111
3 mm Glazing	47.8552791
4 mm Glazing	48.00690072
5 mm Glazing	39.30762567